A Numerical Simulation Study on the Genesis of a Tropical Storm

YOSHIO KURIHARA AND ROBERT E. TULEYA

Geophysical Fluid Dynamics Laboratory/NOAA, Princeton University, Princeton, NJ 08540

(Manuscript received 15 December 1980, in final form 14 April 1981)

ABSTRACT

The genesis of a tropical storm is studied using a numerical simulation model. The model used is an 11-level primitive equation model covering a channel domain of 25° span with open lateral boundaries at latitudes 5.5 and 30.5°N. The initial basic flow field is based on the mean condition at 80°W during Phase III of GATE. The superposed wave disturbance is initially confined in the lower troposphere. The time integration of the model is carried out to 96 h, during which a tropical storm develops accompanied by an upper level anticyclone.

The genetic sequence of the disturbance system, from a shallow easterly wave into a tropical depression and further into a tropical storm, is described. The minimum surface pressure of the system deepens from 1008.4 to 1002.6 mb at 96 h. The maximum surface wind at 96 h is above 17 m s^{-1}. The relative vorticity at 950 mb intensifies from 43×10^{-6} s^{-1} at the initial time to 237×10^{-6} s^{-1} at 96 h. The surface convergence increases from 24×10^{-6} s^{-1} to 71×10^{-6} s^{-1}. The processes involved in the above transformation are extensively discussed. Attention is given to the change in the area of rainfall and cloud from a zonal pattern to a cluster-type, the deepening of the cloud within the system, the appearance of horizontal tilt of the trough axis and the time variation of its vertical tilt, the evolution of the vertical motion field, the thickening of the convergence layer around the depression center, the formation of a warm core at 335 mb and its downward extension, the appearance of a cold core at a higher level, etc. The intensification of the vortex and the growth of a warm core are analyzed by examining the budgets of vorticity and heat at the tropical depression stage. The vorticity increase at low levels is due to stretching of the vortex. Relative horizontal advection causes a decrease of vorticity in some outer areas. At upper levels, the upward protrusion of positive vorticity from below and relative horizontal advection cause a positive tendency. Both the effect due to horizontal divergence and the twisting up of a horizontal vortex make negative contributions. The net effect at upper levels is to produce a compact positive vorticity area within a large region of negative vorticity. Upper level warming is largely due to the excess of the condensation-convection heating over the cooling effect associated with the upward motion. The appearance of an upper level disturbance in the present model is caused entirely by the forcing from below. Supplemental experiments confirm that, although the diabatic heating effect of radiation plays an important role, the heating due to the condensation of water vapor is essential for the formation of a tropical storm in the present case.

1. Introduction

Over the tropical oceans, a weak atmospheric disturbance sometimes develops into a tropical depression, with winds up to ~17 m s^{-1} (33 kt), occasionally to a tropical storm, and in certain cases further to a hurricane or typhoon, with winds of ~33 m s^{-1} (64 kt) or higher. The search for conditions which control the development or non-development of a tropical disturbance is certainly an intriguing subject in tropical meteorology.

Numerous studies have been made to clarify the process of tropical storm formation, but no general mechanism has been accepted. In these studies, various methods were used to treat the complicated phenomenon. Synoptic analysis is useful for depicting in detail a process of evolution of a particular tropical storm (e.g., Yanai, 1968). A compositing technique is applied to a collection of data for many cases in the hope that common basic features of storm formation will be detected [e.g., Gray (1979) where many observational studies are referred to]. Climatological or statistical analysis is made mainly for finding a correlation between a climatological parameter and storm occurrence (e.g., Gray, 1968). Theoretical studies on the behavior of finite-amplitude waves add to our understanding of the tropical storm genesis (e.g., Shapiro, 1977). Besides the observational or theoretical analyses, another way to approach the problem is the use of a numerical model of a tropical disturbance. An advantage of a model study, both diagnostic and prognostic, is that we can specify atmospheric conditions at our disposal. Also, we can conduct a quantitative discussion based on the numerical results of a model.

We summarize in the following discussion the conditions which were suggested by studies in the past as favorable for or related to the formation of tropical storms:

1) Warm sea surface temperature. Palmén (1948) pointed out that a disturbance may develop when the sea surface temperature over a large area is higher than 26–27°C. Effects of the area size of warm water (Wendland, 1977) and of the ocean thermal energy, i.e., sea temperature to a depth of 60 m (Perlroth, 1969; Gray, 1979), on the storm formation were discussed. Warm sea surface temperature contributes to a high equivalent potential temperature in the atmospheric boundary layer.

2) Preexisting low-level disturbance. At some time in the past, a source of hurricanes and typhoons was sought in the lower tropospheric waves in the tropical easterlies (Dunn, 1940; Riehl 1948, 1954; Palmer, 1952). Actually, statistics indicate that a majority of Atlantic depressions develop either from the easterly waves originating over Africa or the disturbances along the intertropical convergence zone (e.g., Frank and Clark, 1979).

Synoptic analysis of the particular disturbances by Yanai (1961a), Hawkins and Rubsam (1968) and Vincent and Waterman (1979) revealed the existence of large-scale vertical motion and low-level confluence in the waves which later developed into tropical storms. Recently, compositing methods have been used by many investigators to analyze the structure and behavior of the easterly waves over Africa and the eastern Atlantic (Burpee, 1972, 1974, 1975; Pedgley and Krishnamurti, 1976; Reed *et al.*, 1977; Norquist *et al.*, 1977; Shapiro, 1978; Nitta, 1978; Reed, 1979; Murakami, 1979; Thompson *et al.*, 1979; Stevens, 1979), and those over the central and western Pacific (Reed and Recker, 1971; Reed and Johnson, 1974). Miyakoda *et al.* (1980) made a four-dimensional analysis of GATE (GARP Atlantic Tropical Experiment) data to discuss the transient features of easterly waves. Sometimes, tropical storms are initiated in the upper troposphere and propagate downward (Ramage, 1959; Cochran, 1976).

3) General warmth in 500–200 mb layer. The appearance of an upper level warm area in the formation process of tropical storms is commonly observed.

The warming is often associated with organized convective activity (e.g., Yanai, 1961a, b, 1964; Fett, 1966a; Hawkins and Rubsam, 1968; Leary and Thompson, 1976). Ceselski (1974) suggested the importance of "persistability" of convection. Although the convection is even regarded as a necessary part in the storm formation process (Frank, 1963), Riehl (1967) argued that the mesoscale structure of clouds might inhibit the intensification of waves. Based on their model study, Estoque and Cheng (1974) pointed out a possible role of large-scale non-convective rain at an early stage of wave development.

Another cause of the upper level warming may be the downward motion related to the upper level shear zone (Yanai, 1968). Gray (1979) considers a dynamically forced subsidence to be a necessary requirement for the genesis.

4) Upper level disturbance. It has been noticed by many investigators that a divergent, anticyclonic flow at upper levels appears to be favorable for the development of the low-level disturbances in the tropics (e.g., Riehl, 1948; Colón and Nightingale, 1963). According to Gray (1979), the difference of vorticities between 200 and 900 mb levels gives a measure for the daily genesis potential. Yanai (1963) stated that the weak absolute vorticity at upper levels together with the warming of middle-tropospheric air is an almost necessary and sufficient condition for the development of a wave disturbance into a typhoon. He noted that the superposition of an upper level anticyclone and the middle-level warming might not be completely independent phenomena. In the observational analysis by Hawkins and Rubsam (1968), the above two phenomena were coincidental. Frank (1963) and Fett (1966a) treated the cases in which the upper anticyclone was apparently caused by the latent heat release through cumulus convection. As suggested by Ceselski (1974), the evolved upper level flow may play a role in the maintenance of convection.

Upper level troughs also are considered to affect the evolution of low-level tropical disturbances. The development of a wave into a tropical storm may be triggered by a sharpened overlying trough (Ramage, 1959). Sadler (1976, 1978) discussed a possible role of the tropical upper tropospheric trough over the Pacific in the intensification of a low-level system. Yanai (1968) analyzed a case in which the interaction between a low-level disturbance and a pronounced upper level shear line initiated a secondary system. On the other hand, Simpson *et al.* (1969) noted an apparent effect of the upper tropospheric trough or shear line to subdue the incipient disturbances. In addition, large-scale disturbances of the upper air outside the tropics may interact with those inside the tropics. Riehl (1950) conjectured that such an interaction may cause mass divergence at high levels and contribute to the initial phase of hurricane formation.

5) Favorable basic field. Thermodynamically, formation of a tropical storm is connected with the ubiquitous conditional instability of the air in the tropics (Palmén, 1948). Shukla (1969) made a numerical study to see the dependency of the behavior of easterly waves on the Richardson number.

The basic flow surrounding a disturbance is gen-

erally not uniform. Gray (1968) stated that horizontal cyclonic shear at low levels was a favorable factor for the storm formation. Agee (1972) connected the cyclonic shear to the breaking of a wave and the formation of a vortex. Shapiro (1977) derived a formation criterion which measures the contribution of nonlinearity in the dynamics of finite amplitude waves. Empirically, his criterion is related to the horizontal nonuniformity of the mean flow.

The mean flow field may become barotropically unstable. Nitta and Yanai (1969) discussed the barotropic instability of a sine-profile easterly jet and showed the possibility of instability over the western Pacific. The behavior and structure of the unstable barotropic waves on the sine-profile jet were investigated by Yamasaki and Wada (1972a, 1972b). Lipps (1970) and Dickinson and Clare (1973) examined the barotropic instability of mean flow with hyperbolic-tangent shear. Those perturbation-type stability analyses may be applicable to the wave stage of storm formation.

The vertical shear of the mean flow varies both in space and time in the tropics. Using his diagnostic model, Holton (1971) showed that the structure of easterly wave is quite sensitive to the vertical shear. He also suggested that the waves may rather quickly adjust to the condition of local mean wind. The vertical shear causes differential vorticity advection, which, under the quasi-balance assumption, affects the vertical motion in the wave. This effect was pointed out by Yanai (1961b) and Krishnamurti and Baumhefner (1966).

The vertical shear is also connected to the ventilation, i.e., removal of heat above a low-level disturbance by the wind relative to a moving disturbance. In this respect, Gray (1968, 1979) considered a weak vertical shear favorable for the storm formation.

6) Other factors. A tropical storm is rarely formed near the equator. As suggested by Palmén (1948), the contribution of horizontal convergence to a vortex development is weak in the equatorial area because of a small value of the Coriolis parameter.

The behavior of a disturbance may be affected by the cloud-modulation of radiational heating. Large-scale forced response of the waves in the tropics to such a modulated heating was studied by Albrecht and Cox (1975) using a diagnostic model. In a prognostic study, the increased development of disturbances over the ocean was noticed in the presence of clouds (Slingo, 1978).

Recently, the possible significance of cumulus friction in a formation process was pointed out (Gray, 1979; Mak, personal communication). If the unbalance between the mass and momentum fields occurs, the mechanism of geostrophic adjustment (e.g., Schubert *et al.*, 1980) will operate.

It seems that the above summary indicates a great variety of involved features associated with tropical disturbances and their development. After all, it is not easy to delineate a disturbance within the context of the large-scale environment, especially at an incipient stage. In the present study, we treat the problem of tropical storm genesis with a numerical simulation model. Our model uses a parameterization method to incorporate the thermodynamical effect of cumulus convection. The validity of using a parameterized model for our purpose is not beyond question. However, its usefulness in its own degree was hinted in the earlier work by Manabe *et al.* (1970). Also, the prognostic results from the parameterized models by Miller *et al.* (1972) and by Ceselski (1974), in which both developing and non-developing systems were treated, were encouraging. We design our experiment so that an instructive, basic case is presented. Specifically, each of the conditions listed before is taken into consideration as follows: (i) reasonably warm fixed sea surface temperature; (ii) a simple, shallow easterly wave at the initial time; (iii) no upper tropospheric warm area at the initial time; (iv) no upper level disturbance at the initial time; (v) a simple initial basic state which is presumably favorable for the development of a disturbance, and (vi) a domain avoiding the equator and the incorporation of radiation effect. Initial conditions for both basic flow and a wave are deliberately made simple. In particular, we emphasize the absence of the conditions (iii) and (iv) at the start of the time integration. The wave is not initially accompanied with cloudiness, but will give rise to it as the integration proceeds. The whole system is expected to be nearly self-contained within the model domain during the integration.

In this paper, the numerical model used and its initial conditions are described in Sections 2 and 3, respectively. Evolution of the flow field, from a wave to a storm, is presented in Section 4. In Section 5, transformation of wave to a depression stage is analyzed. Vorticity and heat budgets of a tropical depression are estimated in Section 6, and the further development of a system into a tropical storm is elucidated in Section 7. In Section 8, the effects of diabatic heating on the storm formation are discussed based on the results of supplementary experiments. Section 9 contains a summary of the results as well as remarks on the subject of the prognosis of tropical storm genesis in general.

2. Brief description of the model

The numerical model used in this study is a uniform-grid version of the nested-mesh model described by Kurihara and Bender (1980, hereafter referred to as KB) except that the effect of radia-

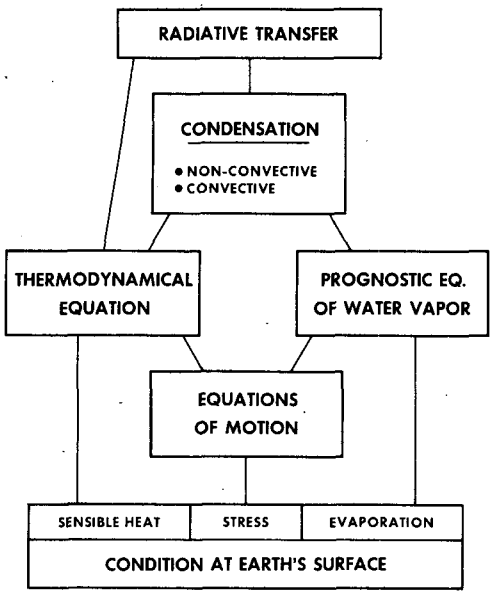

FIG. 1. Diagram showing the system of governing equations and the interrelationship among the components.

tion is included. The nested-mesh model was constructed by modifying and improving certain parts of an earlier tropical cyclone model developed at the Geophysical Fluid Dynamics Laboratory of NOAA (Kurihara and Tuleya, 1974).

The major components of the model and the links among them are schematically shown in Fig. 1. A primitive equation system, that is, the equations of motion, tendency equation, equation for the vertical velocity, hydrostatic relation, thermodynamic equation and equation for mixing ratio of water vapor, governs the model. Adopting the σ-coordinate proposed by Phillips (1957) in the vertical, a spherical coordinate system is used. The model has a channel-type domain with a cyclic condition assumed for its 25° longitudinal span. The lateral boundaries are open (see KB, Sections 2c) and placed at latitudes 5.5 and 30.5°N. The longitude-latitude, non-staggered grid system with a grid resolution of 5/8° in both zonal and meridional direction is used. For studying tropical waves, Krishnamurti *et al.* (1979) considered 1° resolution desirable, while Miyakoda *et al.* (1976) recommended a grid distance of 40 km. The present resolution is in between the above two values. The model atmosphere is divided vertically into 11 layers. Table 1 shows the integer levels, the half-integer levels, which indicate the interfaces between the layers, and their approximate heights. This vertical division is the same one chosen by Kurihara and Tuleya (1974) in their hurricane model.

Subgrid-scale processes in the model are treated by parameterization schemes. The effect of horizontal diffusion is evaluated by the nonlinear viscosity formula, suggested by Smagorinsky (1963). The vertical diffusion process is estimated by the Level 2 formulas of the turbulence closure scheme derived by Mellor and Yamada (1974) (see KB, Appendix A). This formulation is applicable for any stability condition. The so-called dry adiabatic adjustment scheme is not used. The diffusive fluxes of momentum, sensible and latent heat at the sea surface are obtained in the Monin-Obukhov framework (see Kurihara and Tuleya, 1974, Section 3b1). Sea surface temperature is fixed at 302 K. The effect of free moist convection is incorporated in the model through a scheme of moist convective adjustment (Kurihara, 1973; outlined in Kurihara and Tuleya, 1974, Section 3c) with two changes (see KB, Appendix C). It should be noted that this adjustment scheme does not necessarily eliminate the conditional instability entirely.

The effect of radiational heating or cooling is evaluated with a simplified version of the schemes formulated by Lacis and Hansen (1974) and Wetherald and Manabe (1980). In computing this effect, the vertical distributions of temperature and mixing ratio are fixed to a typical condition in the tropics, and only the change in cloud configuration, i.e., existence or non-existence of condensation at each level, is taken into consideration. The profile of radiational cooling is significantly influenced by clouds, but its change due to temperature and mixing ratio fluctuation is considered negligible for this study.

The spatial finite-differencing scheme used in this

TABLE 1. The σ-levels and their approximate pressures and heights.

Level K	σ	Pressure (mb)	Height (m)
0.5	0.00000000		
1.0	0.03060333	31	23637
1.5	0.08318847		17270
2.0	0.12000000	120	14940
2.5	0.17310091		12616
3.0	0.21500000	215	11242
3.5	0.26704077		9847
4.0	0.33500000	335	8328
4.5	0.42025419		6738
5.0	0.50000000	500	5478
5.5	0.59487807		4168
6.0	0.66500000	665	3311
6.5	0.74338763		2424
7.0	0.80000000	800	1843
7.5	0.86092366		1258
8.0	0.89500000	895	926
8.5	0.93042512		575
9.0	0.95000000	950	435
9.5	0.96998671		260
10.0	0.97700000	977	196
10.5	0.98406400		132
11.0	0.99200000	992	68
11.5	1.00000000		0

study is the one explained in KB, Section 2f. The conservation property is satisfied for mass, momentum, internal energy and kinetic energy. Time integration of the model is performed by a two-step iterative method proposed by Kurihara and Tripoli (1976). The two weight values which appear in the formula are set to 0.506 and 2.5 (see KB, Section 2e). As pointed out by Masuda (1978), the above weight values yield very efficient damping of high-frequency noise in a primitive equation model. Additional techniques for reducing numerical noise further are explained in Appendix C of KB.

In case of a prediction with a regional model, the thermodynamical processes which are larger in scale than the domain size cannot be treated unless a precise boundary condition can be specified. Accordingly, a weak constraint may be justifiably imposed on the model to restore a certain variable to its reference value. In the present experiment, the effect of a Newtonian damping such as used by Hayashi and Golder (1978, Appendix B) for the same purpose was incorporated in the prediction of the temperature T after 2 h of time integration. Namely, the damping is made proportional to $\bar{T}(t) - \bar{T}(2)$, where overbar denotes the zonal average and $\bar{T}(2)$ is the average at 2 h, except that $T(t) - \bar{T}(2)$ is taken within six grid rows from the lateral boundaries. The effect is estimated by an implicit scheme with the damping time 24 h. Time integration of the model proceeds to 96 h with a 90 s time step.

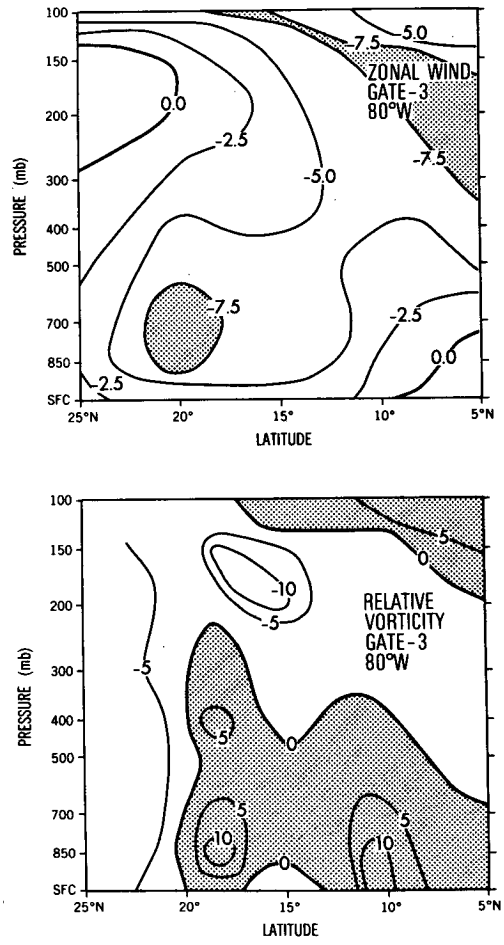

FIG. 2. Latitude-height distributions of the time average of zonal wind (top, m s^{-1}) and the corresponding relative vorticity (bottom, 10^{-6} s^{-1}) for Phase III of GATE, at 80°W.

3. Initial conditions

a. Basic flow

As mentioned in Section 1, we specify a simple, initial basic flow which is expected to be favorable for a superposed disturbance to grow. This is done by idealizing an observed environmental flow condition in which formation of tropical storms were observed. During Phase III of GATE (30 August–19 September 1974) two storms (Carmen and Fifi) formed at ~17°N in the Caribbean. The origin of these storms was an African wave (Frank, 1975). In Fig. 2, the cross sections along 80°W of the zonal component of wind, averaged over the above period, as well as of the relative vorticity computed from it, are shown. The zonal wind distribution is characterized by a very weak shear, horizontally at about the 400 mb level and vertically at about 13°N and an easterly vertical shear in the southern part and a westerly vertical shear in the northern domain. In accordance with the zonal flow mentioned above, the relative vorticity is generally positive below the 400 mb level and negative above it, as shown in the lower part of Fig. 2. Comparing this distribution with the analysis results of the vorticity field in the GATE period obtained by Miyakoda *et al.* (1980), we can guess that the low-level vorticity maximum at ~18°N is associated with easterly waves and that at 10°N represents the intertropical convergence, shear zone.

We assume that the fields such as shown in Fig. 2 provide a propitious condition for storm genesis. It is noted here that a mean observed field is likely to include a consequence of storms to a certain degree. The initial basic flow in the present model is determined from

$$\bar{u}(\sigma, \phi) = -u_1(\sigma) \tanh\left(\frac{\phi - \phi_0}{D}\right) + u_0 \frac{\cos\phi}{\cos\phi_0}, \quad (3.1)$$

where ϕ is the latitude, ϕ_0 the center latitude (18°N) of the channel and D is specified as 2.5° latitude. The horizontal shear in this case is confined mostly within ~400 km on both sides of the center latitude. We set u_0 to -5 m s^{-1}. With $u_1 = 3.75$ m s^{-1} at the lower levels, $u_1 = -3.75$ m s^{-1} at the upper levels,

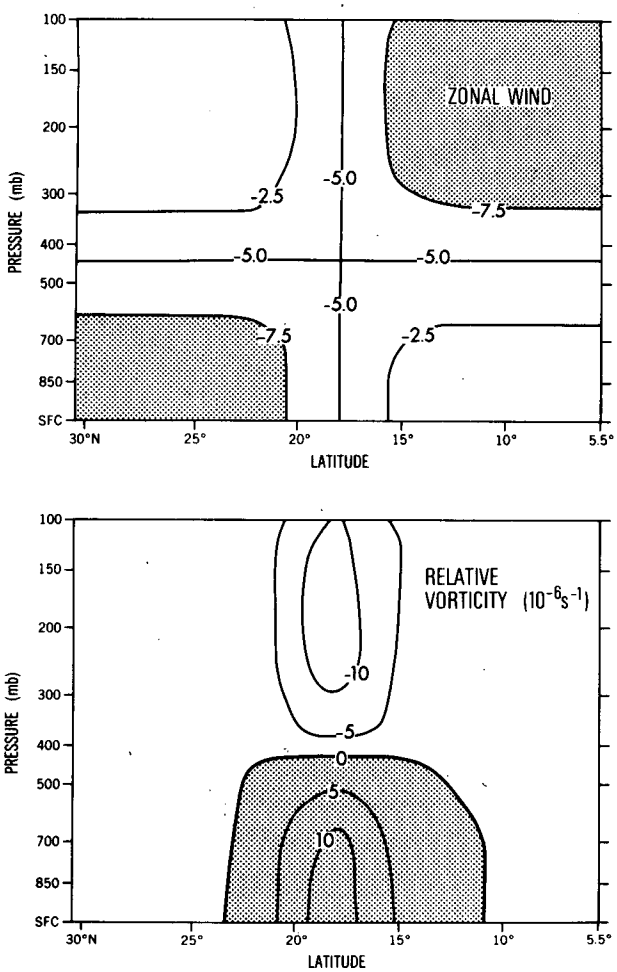

FIG. 3. Latitude-height distributions of the idealized basic zonal flow (top, m s^{-1}) and the corresponding relative vorticity (bottom, 10^{-6} s^{-1}).

and smoothly varying in between, the basic zonal wind and its relative vorticity are obtained as shown in Fig. 3. We note that our proposed low-level basic flow would be barotropically unstable for a small perturbation with a length scale comparable with the channel length (Lipps, 1970; Dickinson and Clare, 1973).

Given a basic zonal flow, the surface pressure and the geopotential of the σ-surface at the lateral boundaries at each level can be obtained from the assumption of the geostrophic balance provided that the surface pressure and the temperatures at each level at a certain latitude are specified (KB, Appendix B). The boundary values thus computed will be used as the boundary condition when the reversed balance equation is solved later. Based on the GATE data at 80°W in the Phase III period, we assigned 1010 mb and 218.6, 201.0, 224.7, 246.9, 267.3, 279.7, 288.6, 294.5, 297.5, 299.1, 299.6 K to p_* and T (at levels 1–11), respectively, at 18°N.

b. Initial disturbance

A simple, shallow easterly wave is assumed as an initial disturbance. Its streamfunction takes the form

$$\psi = -A(\sigma)F(\phi)\cos[2\pi L_\lambda^{-1}(\lambda - \delta)], \quad (3.2)$$

where λ and ϕ are the longitude and latitude, respectively; and $L_\lambda = 25°$, $\delta = 0°$ in this study. The factors to determine the amplitude are given by

$$A(\sigma) = \frac{L_\lambda}{2\pi} v_0(\sigma), \quad (3.3)$$

$$F(\phi) = \begin{cases} \exp\left[-\frac{9}{2}\left(\frac{\phi - \phi_0}{L_\phi}\right)^2\right] - \exp\left(-\frac{9}{2}\right), & \text{for } |\phi - \phi_0| < L_\phi \\ 0, & \text{for } |\phi - \phi_0| \geq L_\phi \end{cases}, \quad (3.4)$$

where ϕ_0 and L_ϕ are set to 18°N and 8.5°, respectively. The distributions of v_0 in (3.3) against σ and that of F, i.e., the left-hand side of (3.4), against $\phi - \phi_0$ are shown in Fig. 4. The initial disturbance is confined below $\sigma = 0.365$ and within 8.5° latitude range from the center of the channel. Its trough axis tilts neither horizontally nor vertically. The decrease of wave amplitude with height implies, under the assumption of a balanced condition, lack of a cold core structure. In this respect, the present disturbance resembles certain waves observed in the Pacific (e.g., Palmer, 1952) more closely than those in the Atlantic.

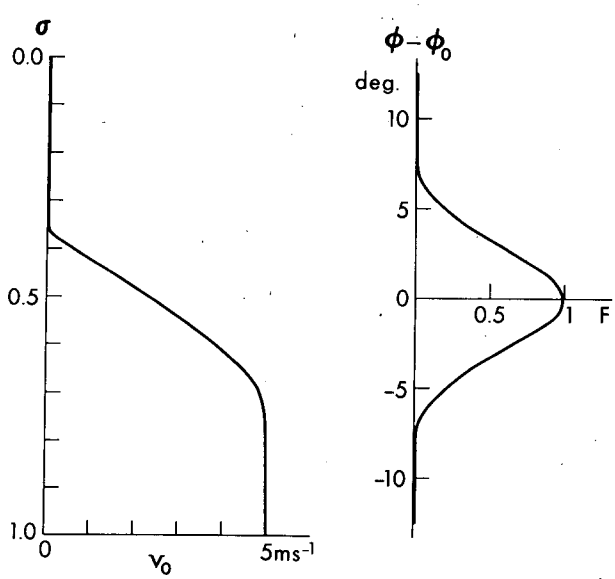

FIG. 4. Vertical variation of v_0 (left) and meridional variation of F (right). These parameters determine the amplitude of the initial wave disturbance.

Superposing the disturbance flow on the basic flow, we obtain the total wind field. The corresponding mass field is given by the solution of the reverse balance equation. The pressure at the lateral boundaries, which were estimated before, provides the boundary condition for the relaxation procedure (KB, Section 3 and Appendix B).

c. Temperature and moisture fields

The temperature field is easily derived from the pressure field through the hydrostatic relation. The temperature at the sea surface is fixed at 302 K, as mentioned before.

The mixing ratio of water vapor is computed from the temperature and the relative humidity which we specify at each level. Using the mean relative humidity data for the GATE Phase III period at 80°W, we specify 10, 20, 30, 38, 51, 61, 71, 78, 82, 83 and 84% to the 11 levels, from the top to the bottom, respectively. Values at the three upper levels are assigned. The observed data indicate that the humidity was quite high to a large depth at the above longitude and period compared with the moisture at the other longitudes and other periods of GATE.

d. Dynamic initialization

After the static initialization, the dynamic initialization is performed in order to establish a reasonable profile of the wind in the planetary boundary layer through frictional adjustment. Existence of the boundary-layer convergence or divergence of the air in the model at the initial time seems desirable rather than its probable evolution in the course of integration. The dynamic initialization is made by a scheme proposed by Kurihara and Tuleya (1978) and supplemented by Kurihara and Bender (1979). Specifically, the model is integrated with the addition of artificial forcing for 12 h without changing the whole mass field and the wind field above the level 9. The initialization of the model is complete at this point.

4. Evolution of wind and surface pressure fields

In this section, the evolution of wind and surface pressure fields during the entire integration period is described. The flow fields at 0, 24, 48, 72 and 96 h are represented in the columns in Fig. 5. Each column consists of four frames showing the streamlines and isotachs for a subdomain (an area between latitudes 11 and 29°N and a longitude range of ~18°) at levels 2 (~120 mb), 4 (~335 mb), 8 (~895 mb) and 11 (~992 mb).

At the initial time, the disturbance is confined to the lower levels. Accordingly, the wind at levels 2 and 4 is the basic zonal flow with an anticyclonic horizontal shear. At level 8, a wave without tilt of axis is present. The backing of wind with decreasing height and the convergence at level 11 are a result of the dynamic initialization, reflecting the effect of the surface stress. At 24 h, the upper level flow is still almost zonal. The wave at level 8 exhibits a northeast-to-southwest tilt of the wave axis, which is a generally observed feature of an easterly wave and suggests the northward transport of westerly momentum by a wave. The convergence at the lowest level increases. The wind field at 48 h indicates a forced change in the upper level flow. At level 2, the speed of the easterlies in the southern area exceeds 10 m s^{-1}. An appearance of a wind pattern with anticyclonic curvature in the northern portion and a weak sign of cyclonic curvature in a small central area over the surface disturbance are the features at level 4. At the lower levels, a nearly circular flow is formed in the region of wave crest. Also, a weak cyclonic flow is noticed in the vicinity of the southwestern corner of the frame. The above-mentioned characteristics at 48 h become more evident at 72 h and increasingly so at 96 h. At level 2, an anticyclonic flow develops and the speed of the easterlies in the southern area is locally above 15 m s^{-1} at 96 h. The position of the anticyclone is shifted to the north of the center of the low-level vortex. Such a meridional phase shift was obtained by Holton (1971) in his diagnostic model. The wind at level 4 is anticyclonic in general, but the flow in a small area right above the low-level vortex is cyclonic. At levels 8 and 11, the primary vortex becomes compact and stronger. An elongated area of strong wind is situated north of the vortex. Such a wind pattern is often observed in the earlier stage of wave evolution (e.g., Yanai, 1961a). The maximum wind speed at level 11 is above 17 m s^{-1} at 96 h. We are now able to state that a tropical storm is formed in our model. A secondary cyclonic flow mentioned before develops into a somewhat large but weak distinct vortex.

Fig. 6 shows the evolution of the relative vorticity field at level 9 (~950 mb). The vorticity fields, together with the positions of the wave trough at the surface shown by solid lines, at 12 h intervals are presented. In the present paper, if a disturbance system has a corresponding minimum in the sea surface pressure, its position is indicated in a figure by a cross mark. Otherwise, the position of the relative vorticity maximum on level 9 is marked by an open circle. Time series maps are prepared by shifting a drawing area within the channel so that the major system, denoted by A, locates nearly on the central longitude of the area.

There exist three vorticity maxima at level 9 at the initial time (Fig. 6a), of which only the major system A has an associated minimum in the sea level pressure field. Two systems B and C are present

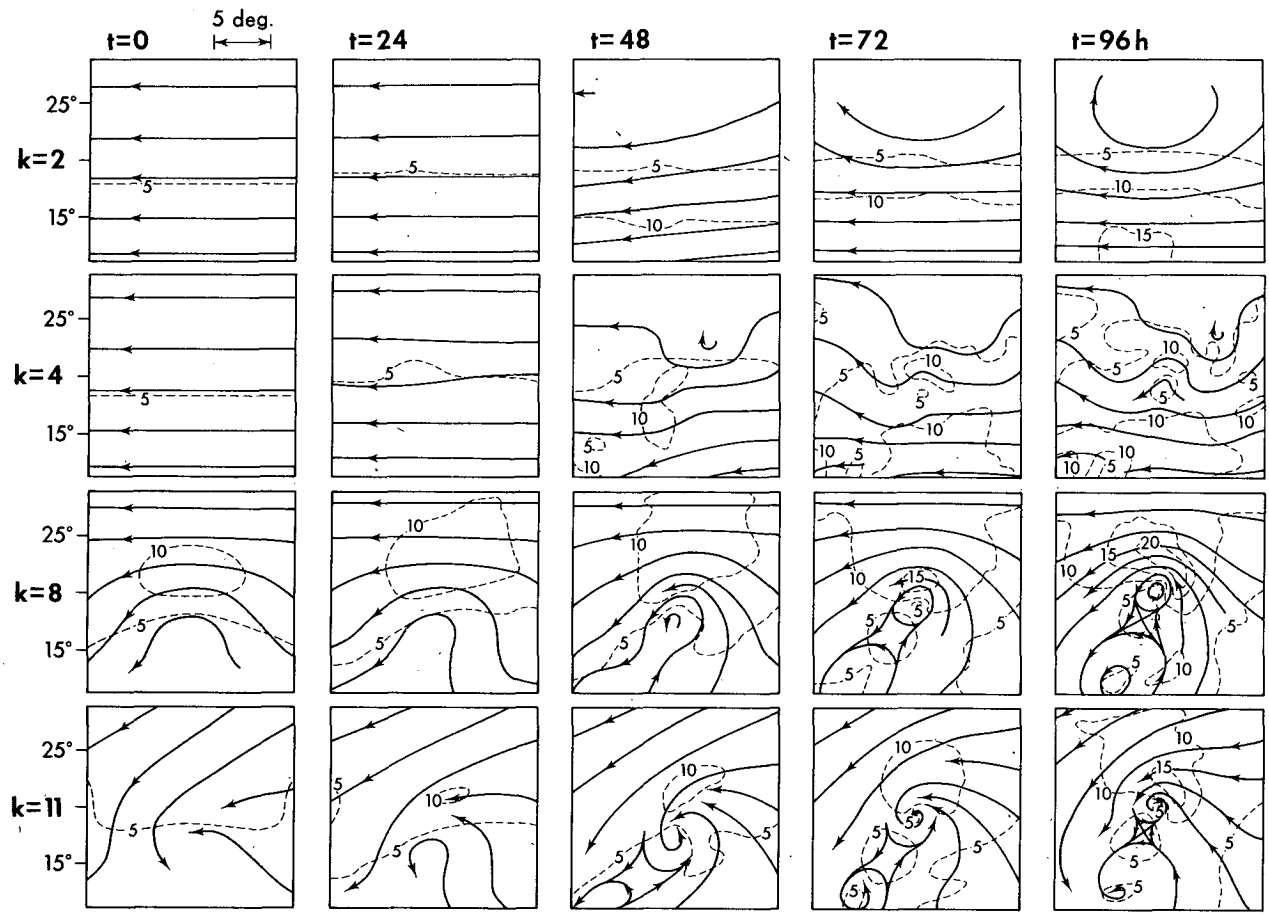

FIG. 5. Streamlines and isotachs (m s^{-1}) at levels 2, 4, 8 and 11 (from top to bottom in each column, at 0, 24, 48, 72 and 96 h (from left column to right).

because of the particular functional form assumed in (3.4). The maximum intensity of the initial vorticity of the system A is 43×10^{-6} s^{-1}. This value is comparable with 45×10^{-6} s^{-1} which is the estimate at 700 mb level by Yanai (1961a) in the wave stage of a typhoon formation. Vorticity maxima of the systems B and C are 7×10^{-6} s^{-1}. System A gradually develops into a nearly circular pattern at about 60 h. In Yanai's case mentioned above, the vorticity increase in 36 h in the wave stage was 50%. In our case, it is 70%. Before 48 h, the vorticity distribution shows an elongated pattern, and the positions of vorticity maximum and surface pressure minimum are not close. These two locations nearly coincide as the system intensifies. The vorticity maximum at the tropical storm stage is ~250 $\times 10^{-6}$ s^{-1}. The negative vorticity is generally greater than -20×10^{-6} s^{-1}, and is never reduced below -30×10^{-6} s^{-1} at level 9. System B is barely identifiable at the beginning. It develops slowly and the corresponding surface pressure minimum appears at 48 h. In the present study, the analysis is focused on the evolution of system A. System B seems to have a potential to grow faster, depending on the environmental condition. This will be a subject for future study. System C which is present at the initial time loses its identity quickly after the start of the integration.

Time series maps of the divergence field at level 11 (~992 mb) are shown in Fig. 7. The general pattern of the divergence field is highly similar to that of the vorticity field at each time level. A large positive vorticity at level 9 (roughly at the top of the boundary layer) is associated with a strong surface convergence. A divergence field at the initial time is due to the dynamic initialization of the wind field in the boundary layer. Maximum convergence thus obtained is 2.4×10^{-5} s^{-1}. At 12 h, an area of strong convergence is east of the surface trough. It shifts onto and in the vicinity of the trough at 36 h. After that, the pattern of divergence field gradually changes from a zonal belt to clusters. The maximum convergence at 96 h is 7.1×10^{-5} s^{-1}.

Fig. 8 shows the time variation of the surface pressure field. At the initial time, the trough has no tilt. The north-northeast to south-southwest tilt ap-

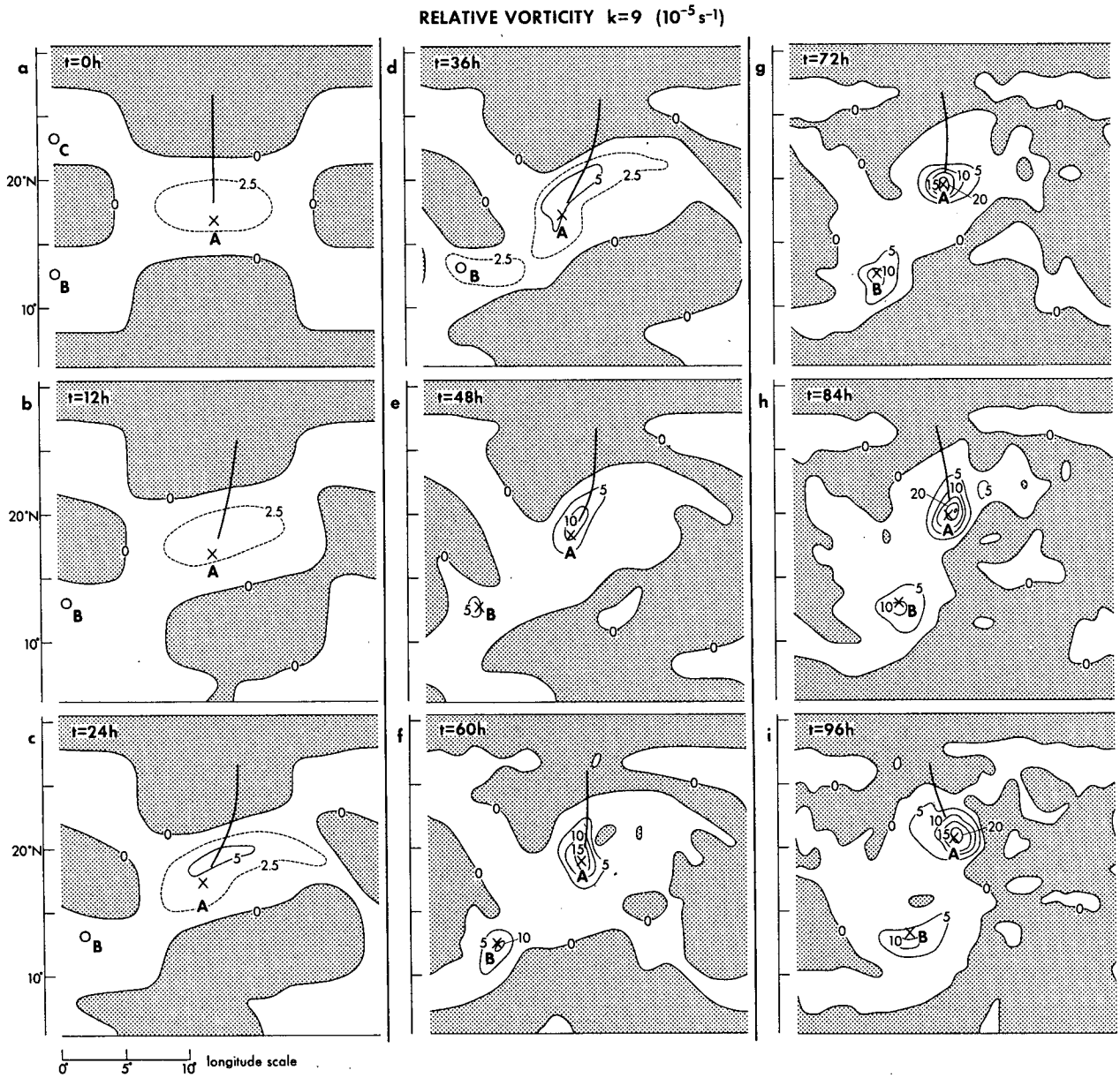

FIG. 6. Distribution of relative vorticity at level 9 (10^{-5} s^{-1}), at intervals of 12 h between 0 and 96 h (a)–(i). Shaded areas denote negative values. Solid lines indicate position of surface trough. Cross marks show the position of systems having a surface pressure minimum and open circles show those without it.

pears quickly after the start of the time integration. The direction of tilt changes with time after 60 h. The minimum pressure of the system A develops from 1008.4 mb at 0 h to 1002.6 mb at 96 h. The system B shows its surface pressure minimum only after 48 h.

As mentioned before, Figs. 5–8 are prepared by shifting the reference frame in a cyclic channel. Actually, the system A propagates westward with an average speed of 6° longitude day^{-1}, which is larger than the average speed of the easterlies, i.e., ~4° longitude day^{-1}. Also, it has a northward component of 1° latitude day^{-1}. Propagation of the system B also is westward with an average speed of ~4° longitude day^{-1}.

5. Transformation processes from an easterly wave to a tropical depression

A tropical depression is often defined as a disturbance having a closed isobar near the wave crest in the surface pressure map. Such a state is observed at 36 h in the present experiment. In this section, the structural change of the disturbance

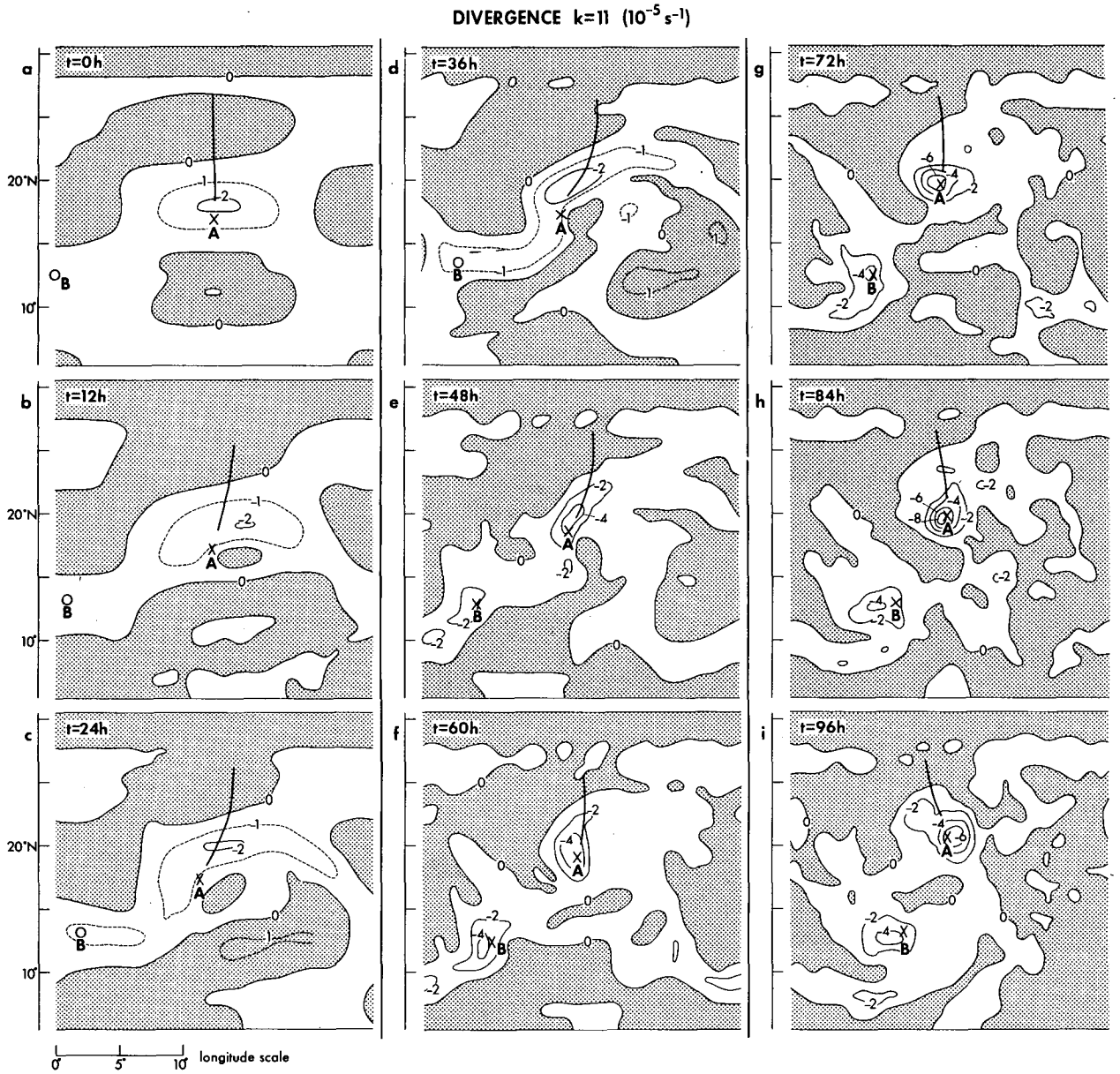

FIG. 7. Distribution of divergence of wind at level 11 (10^{-5} s^{-1}), at intervals of 12 h between 0 and 96 h (a)–(i). Shaded areas denote positive values. See Fig. 6 for further information.

during the period of transformation from an easterly wave to a tropical depression is investigated.

In Fig. 9, the distributions of the rainfall intensity at 12, 24 and 36 h and those of the cloud top, which is defined as the highest level being affected by the condensation of the water vapor, are presented in the left and right columns, respectively. In the left column, the isobars at the surface and the location of the trough at the surface (solid line) and at level 7 (~800 mb) (broken line) also are drawn.

At 12 h, the precipitation area with an intensity > 0.4 mm h^{-1} extends zonally north of the surface pressure low. The rain is very light and the maximum intensity is only 0.5 mm h^{-1}. The clouds are at low levels everywhere. By 24 h, the rain intensity increases to 2.3 mm h^{-1}, i.e., a moderate level, at and in front of the trough, with light rain extending well to the east of it. Middle-level clouds are distributed zonally across the trough line. Clouds reach level 4 at and in front of the trough. Over the surface low, the clouds are low and the precipitation is very weak. The rain and the cloud patterns at 36 h differ from those at the earlier times.

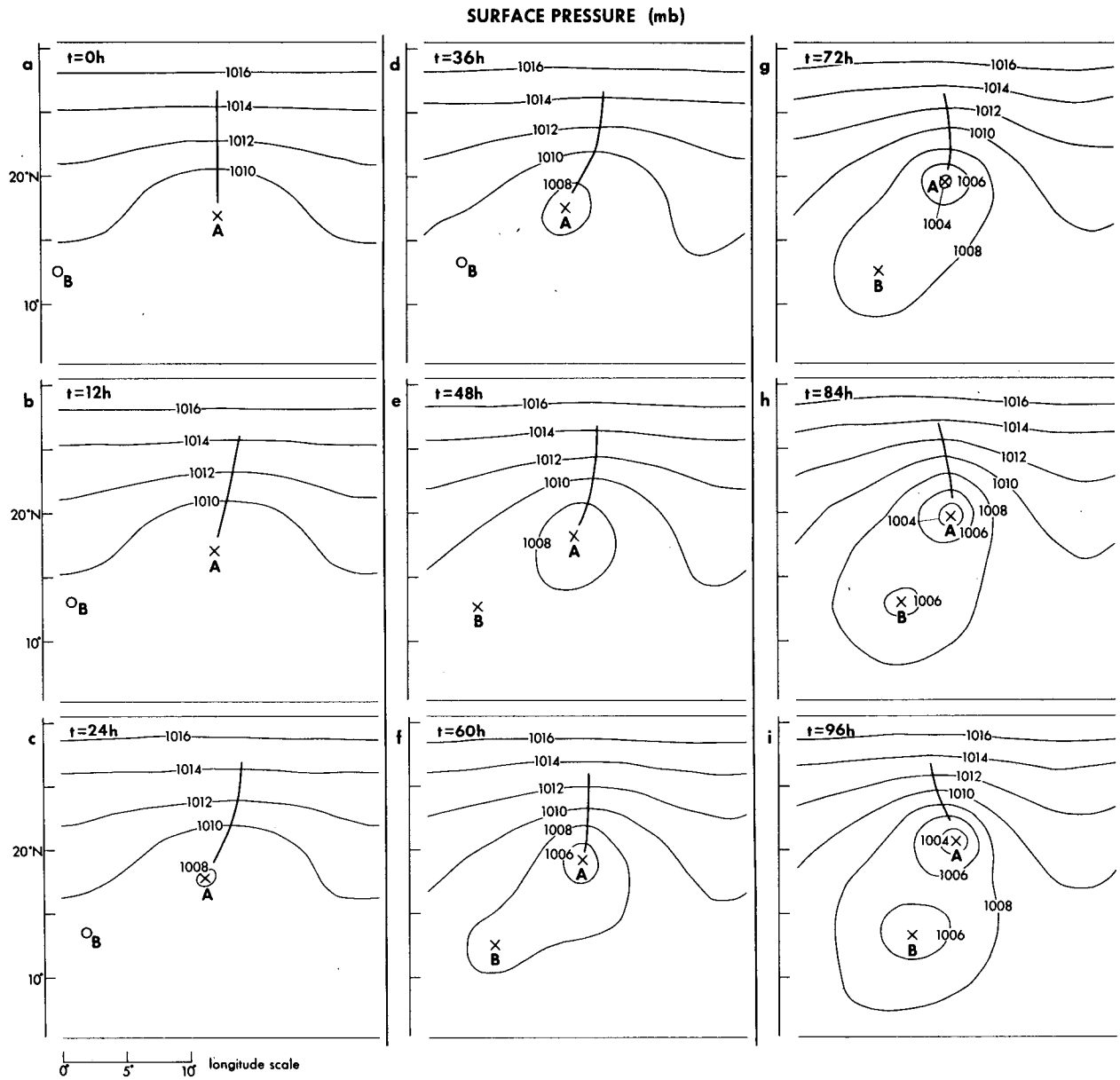

FIG. 8. Distribution of surface pressure (mb), at intervals of 12 h between 0 and 96 h (a)–(i). See Fig. 6 for further information.

The area of moderate rain, with the maximum intensity 4 mm h^{-1}, extends to the west of the depression. Thus, a relatively intense rain zone to the north of the vortex tilts in a west-southwest to east-northeast direction. The high cloud region more or less coincides with the moderate precipitation area. Clouds show some tendency to change pattern from a zone-type to cluster. At the center of the depression, the rain is still light.

Observationally, either an amorphous mass of clouds (Hawkins and Rubsam, 1968), an inverted "V" cloud pattern (Simpson *et al.*, 1968; Frank, 1969) or a minor wave pattern (Thompson and Miller, 1976) is often detected at the very early stage of tropical disturbances. Clouds which appear in the present model seem to belong to a category of minor waves. As an easterly perturbation develops, the cloud distribution takes a vortical pattern (Merritt, 1964). This tendency is seen in Fig. 9. Comparison of the figures at the same time level in Figs. 6 and 9 indicates a high correlation between the relative vorticity at level 9 and the distributions of precipitation and cloud. The position of the surface low is off the area of major convective activity. Fett (1966b) noted that the main overcast area in the weaker stage of depressions does not

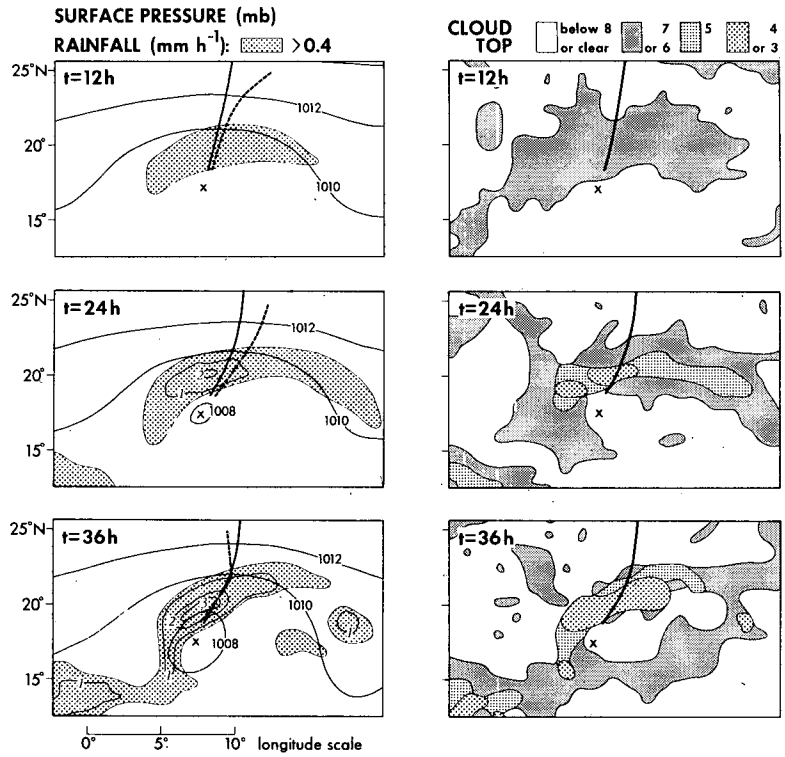

FIG. 9. Distribution of surface pressure (mb) and rainfall intensity (mm h^{-1}) (left) and level of cloud top (right), at 12 h (top), 24 h (middle) and 36 h (bottom). Heavy solid and dashed lines indicate the positions of trough at surface and level 7, respectively. Locations of surface pressure minimum are shown by cross marks.

coincide with the apparent center of circulation determined from the satellite photographs of clouds. The rainfall and cloud distributions at 36 h in Fig. 9 suggest a similar feature.

The left column in Fig. 9 shows that the trough axis at level 7 (~800 mb) in the model is located to the east of the surface axis at 12 and 24 h, but by 36 h the troughs coincide. The above change in the vertical tilt of the trough axis agrees with the analysis result obtained by Reed and Recker (1971) for the waves in the western Pacific. Namely, the axis of these waves changes its tilt from eastward with increasing height, to straight vertical and finally to westward as the waves move westward. Rainfall in the present model is large near or ahead of the surface trough. Such a distribution has been suggested for certain waves in the Pacific (Palmer, 1952; Reed and Recker, 1971) and for some disturbances in the Atlantic (Merritt, 1964). It is different from the case of open easterly waves in the Atlantic (Riehl, 1954).

In this study, the convective activity, which is expressed in a parameterized manner, persisted in the trough region throughout the early transformation period. Ceselski (1974) stressed the persistence of convection as an important factor for a storm formation. Continuous destabilizing effects, which should oppose the stabilizing effect due to convection, can be expected from the large-scale vertical motion, the radiation, etc. Nitta (1978) noticed a high correlation between the observed low-level cloud and the vertical p-velocity ω near the cloud base.

In Fig. 10, the distributions of the vertical motion and the temperature deviation from an arbitrary constant value at levels 3 (~215 mb), 4 (~335 mb) and 7 (~800 mb) are presented for the time levels 12, 24 and 36 h. It is seen that the low-level clouds (Fig. 9) are certainly correlated with ω at level 7.

Generally speaking, the temperature field is much smoother than the ω field, at all three time levels. At 12 h, ω at level 7 is primarily related to the boundary-layer convergence (Fig. 7b). The maximum upward motion of the order 1 cm s^{-1} is obtained at ~2° latitude north of the surface low. It is interesting to note that the pattern of ω distribution is reversed from levels 7 to 4, meaning the existence of a nodal level of ω in between these two levels. At level 3, ω is negligible. The maximum magnitude on this level is only 0.08 cm s^{-1}. A very weak warm area shown on level 7 reflects a mass field balanced to the initial disturbance which has a decreasing amplitude with height (Fig. 4, left). By 24 h, the upward motion to the

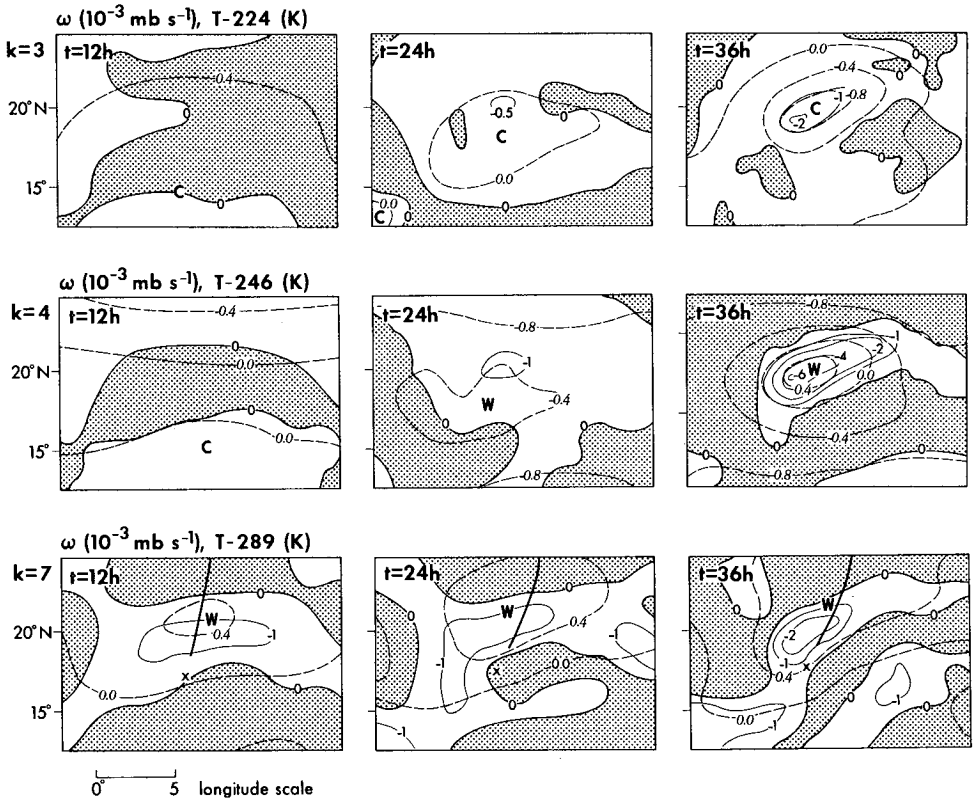

FIG. 10. Distribution of vertical p-velocity (10^{-3} mb s^{-1}, with shading for positive values) and deviation of temperature from appropriate value (dashed lines, K) at levels 3, 4 and 7 (from top to bottom in each column), at 12 h (left column), 24 h (center) and 36 h (right).

north of surface low penetrates to level 3. The magnitudes of ω at levels 4 and 7 are about the same. This implies the thickening of the convergence layer. A relatively warm region appears at levels 4 and 7, but it is wide and weak. The air in the large part of the warm area is ascending. At level 4, however, the southwestern region of the warm air is sinking. At level 3, a cold area is formed in the region of upward motion. The field of ω changes drastically after 24 h. The maximum upward motion at level 4 at 36 h is 6 cm s^{-1}, while that at level 7 is 2 cm s^{-1}. Further deepening of the convergence layer is evident. On the other hand, the descending motion is very weak. It is strongest at level 7, but the maximum value is only 0.4 cm s^{-1}. The strong upward motion located to the north of the surface depression is in phase with a somewhat concentrated warm core at level 4 and with an intensified cold area at level 3. The temperature of the warm core is about 1 K higher than the surrounding area. At level 7, the warm region is broad and open. The spatial scale of temperature variation is larger than that of ω variation at all levels.

In the present model, a perturbation does not exist in the upper troposphere at the initial time, as mentioned before. Accordingly, the evolution of the warm core at level 4 and that of the cold core at level 3 are definitely phenomena forced from below. In this section, we have shown that the development of the above thermal structure is apparently associated with the large-scale ascending motion, which seems to maintain the convective activities along an elongated zone across the trough of an easterly wave. The upward motion in a stable atmosphere contributes to the cold-core formation. To produce a warm core, the effect of diabatic heating is required. The release of latent heat due to the condensation of water vapor plays an important role as shown in Sections 6 and 8. However, one may argue that, because the warm area and upward motion are not exactly in phase at 24 h and before, other mechanisms besides heat of condensation may also play a role in the early stage of upper tropospheric warming.

In the actual atmosphere, there have been many cases in which the formation of the upper level warm area is simultaneous with the occurrence of the low-level convection (e.g., Yanai, 1961a; Hawkins and Rubsam, 1968). In particular, the present simulation result may be analogous to the case analyzed

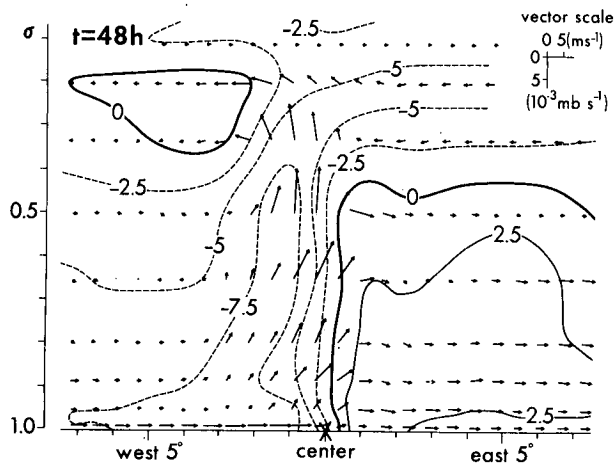

FIG. 11. Longitude-height distribution, through the disturbance center, of the wind relative to the moving system, at 48 h. Arrows represent the zonal and vertical components and isopleths show the distribution of the meridional component (m s^{-1}).

by Frank (1963), in which the convection at the low levels was the entire cause for the appearance of the upper level thermal high.

6. Vorticity and heat budgets of a tropical depression

The tropical depression which evolved in the present model in ~36 h continued to develop during the subsequent time integration. The vortex develops into a compact and intense system. The warm core becomes more pronounced. In this section, we investigate the processes which are responsible for the above changes by making budget analyses of vorticity and heat at the time level 48 h when the tropical depression intensifies more rapidly.

a. Flow relative to the disturbance

The budget analyses are performed in a quasi-Lagrangian manner, namely, the reference frame is fixed to the moving tropical depression. The moving velocity, or phase velocity, is determined from the movement of the position of the surface pressure minimum. At 48 h, its westward component is 6.47 m s^{-1} and northward component is 1.77 m s^{-1}.

Fig. 11 shows the flow field relative to the depression at 48 h on a west–east, vertical cross section which passes through the center of the surface low. The zonal component of the relative wind and the vertical motion are represented by arrows. The meridional component of the relative wind is expressed by contour lines. Since the system moves westward at a speed greater than the basic, low-level easterly wind, the relative wind in the lower trophosphere is eastward. The air flows into the system from the northwest direction. Strong, deep upward motion is located to the west of the center. In the rear of the system, the air flows out to the northeast at the low levels, while it is directed toward the system at the upper levels. Outflow exists at the upper levels toward the front of the system.

In Fig. 12, the azimuthal average of divergence, centered at the depression center, is presented. Within a 3° radius, the convergence layer occupies the lower half of the troposphere and is capped by a divergence layer. The thickness of the convergence layer decreases with the increasing radius. The analysis of actual wind data by Wallace (1971) suggests that most synoptic-scale convergence takes place indeed above the subcloud layer. Also, the appearance of deep convergence was noted in the convective region in the prognostic model by Ceselski (1974). Gray (1979) pointed out the role of deep inflow in the process of storm genesis.

b. Vorticity budget

The rate of change of the absolute vorticity of the moving system may be written in pressure coordinates as

$$\frac{D(\zeta + f)}{Dt} = \mathrm{ZA} + \mathrm{ZB} + \mathrm{ZC} + \mathrm{ZD} + \mathrm{ZE}, \quad (6.1)$$

where

ZA change due to relative horizontal advection $[= -(\mathbf{v} - \mathbf{c})\cdot\nabla(\zeta + f)]$
ZB change due to vertical advection $[= -\omega\partial\zeta/\partial p]$
ZC change due to stretching $[=(\zeta + f)(\partial\omega/\partial p)]$
ZD change due to twisting up of the horizontal component of vorticity
ZE change due to frictional effect.

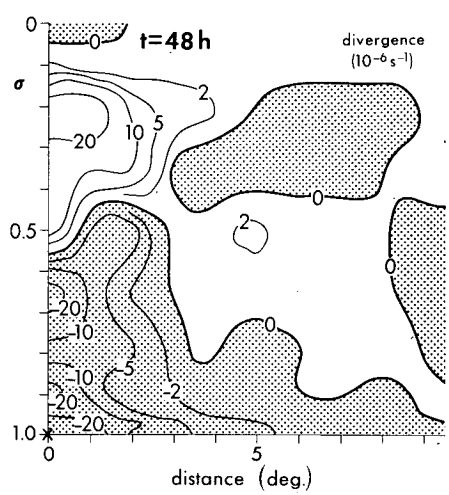

FIG. 12. Height-radius distribution of the azimuthal mean of divergence (10^{-6} s^{-1}) at 48 h, centered at the disturbance center.

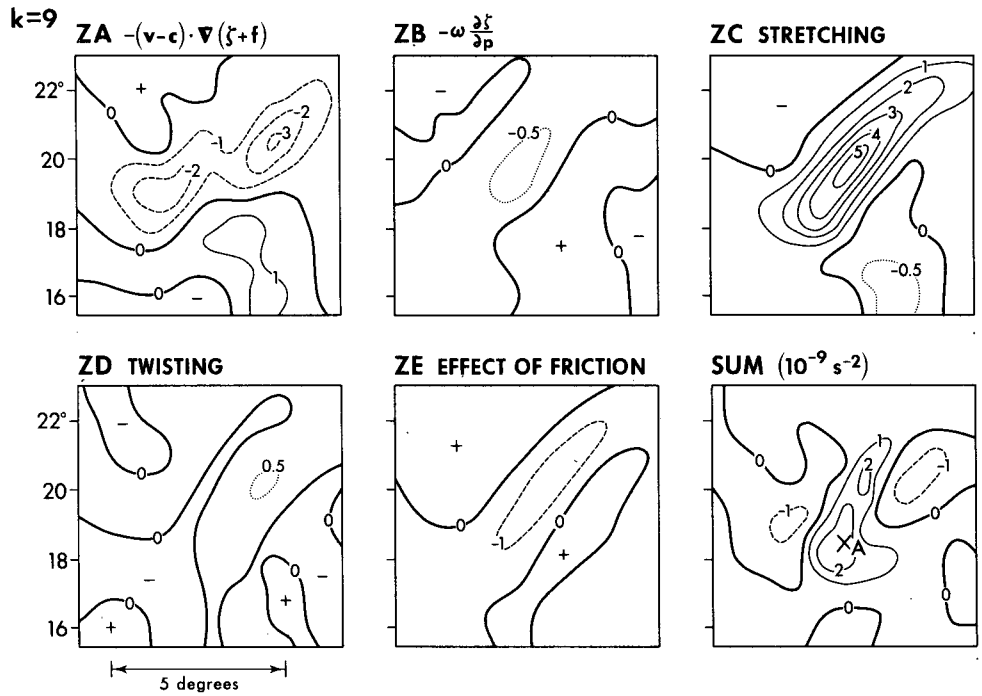

FIG. 13. Distribution of components and sum (10^{-9} s^{-2}) of the vorticity budget at level 9, computed relative to the moving disturbance at 48 h. Cross mark in the lower right figure indicates surface position of disturbance A.

In the above expressions, D/Dt means the change relative to the system which moves with the velocity $\mathbf{c}$, $\mathbf{v}$ is the horizontal wind, ω the vertical p-velocity, ∇ the horizontal gradient operator, ζ the relative vorticity and f the Coriolis parameter.

The distributions of the above budget components and the sum at 48 h on model levels 9 and 4 are presented in Figs. 13 and 14, respectively.

At level 9 (950 mb), stretching of the vortex makes an important contribution to increase the vorticity in the vicinity of the center of the system, the position of which is shown by a cross mark with letter A in the bottom right frame in Fig. 13. The above positive effect is partly canceled by the frictional and vertical advection terms ZE and ZB. The relative horizontal advection term ZA causes a decrease of vorticity in some outer parts of the system. The contribution of the twisting term ZD is relatively small. The sum of all terms indicates a concentration of vorticity through its increase near the center and a general decrease in the surrounding region. The above sum gives the rate of change of the absolute vorticity. The change of relative vorticity, $D\zeta/Dt$, is obtained by subtracting the change of planetary vorticity, i.e., Df/Dt $(=\mathbf{c}\cdot\nabla f)$, from the sum. In the present case, Df/Dt is 3×10^{-11} s^{-2} while the sum is in the order of 10^{-9} s^{-2}. Therefore, the sum is in practical purpose equal to $D\zeta/Dt$.

At level 4 (~335 mb), the term ZA, relative horizontal advection, makes a significant positive change slightly ahead of the system center. This is related to the relative outflow to the front of the system. The upward advection of positive vorticity from below is shown by the term ZB. The negative contribution of ZC is associated with the upper level horizontal divergence of flow as shown in Fig. 12. The twisting effect ZD is related to the vertical shear of wind. The horizontal component of the vorticity vector due to vertical shear is generally pointed outward from the storm center, where the vertical motion is large and upward at this level. Accordingly, the twisting effect produces anticyclonic vorticity. The term ZE, frictional effect, is relatively small. The total tendency causes a compact positive vorticity area to the southwest of surface low in a large background where the vorticity tends to decrease.

The zonal-vertical cross section of $D(\zeta+f)/Dt$, through depression center, is shown in Fig. 15. The zonal and vertical components of the relative flow are also shown by superposed vector arrows. The concentration and intensification of the vortex at all levels in the system is clearly suggested. Also, the formation of negative vorticity in the area surrounding the system, especially at upper levels, is hinted. The association of strong upward motion and positive tendency in Fig. 15 implies the importance of the effects of vertical transport and stretching in the vorticity budget. This agrees with

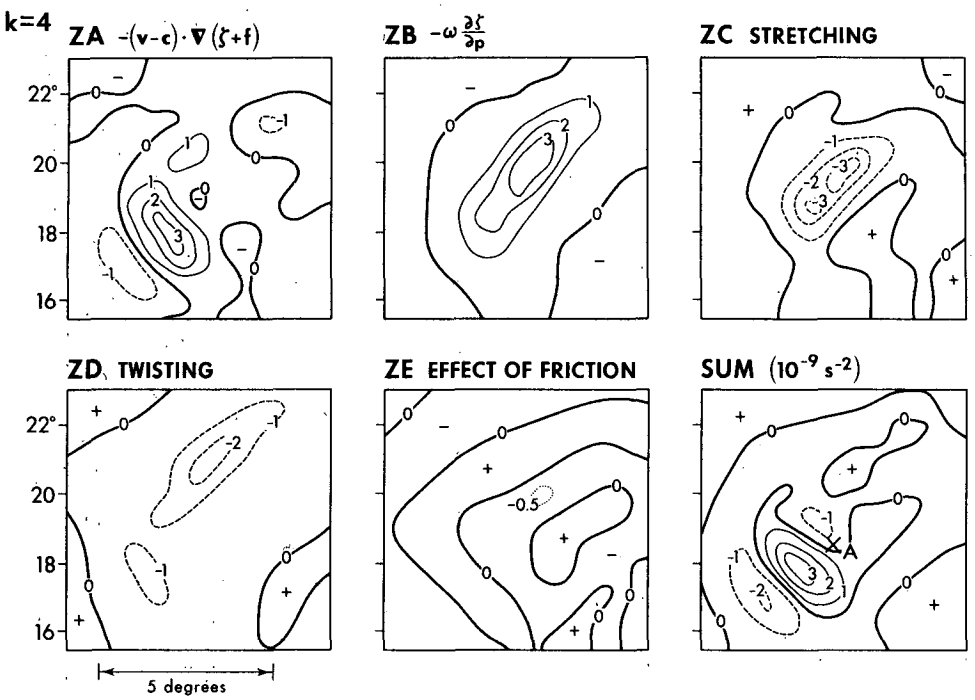

FIG. 14. As in Fig. 13 except for level 4.

the observational analysis of the typhoon at its formative stage made by Yanai (1961a).

The frictional term ZE of the vorticity budget which may include cumulus effects through stability-dependent vertical diffusion is small in the present experiment, and apparently contradicts some observational studies. Vincent and Waterman (1979) obtained a large vorticity source at upper levels in their case study of Hurricane Carmen. Vorticity budget studies of composite waves (Reed and Johnson, 1974; Shapiro, 1978; Stevens, 1979) yield a large residual term which is usually associated with frictional effects of cumulus convection. We cannot make a definite assessment of the frictional effect because we do not know whether this discrepancy is due to improper physical modeling of cumulus transport of momentum or difficulties in computing the vorticity budget from observations. The budget for a composite wave is only significant provided it is equivalent to the average budget for individual waves.

c. Heat budget

The equation for the temperature change on the moving system may be written as

$$\frac{DT}{Dt} = \mathrm{TA} + \mathrm{TB} + \mathrm{TC} + \mathrm{TD} + \mathrm{TE}, \quad (6.2)$$

where

TA change due to relative horizontal advection $[= -(\mathbf{v} - \mathbf{c})\cdot\nabla T]$

TB change due to vertical motion $[= -\omega(\partial T/\partial p - \alpha/c_p)]$

TC change due to condensation-convection

TD change due to radiation

TE effect of diffusion.

The distributions of the above budget components and the sum at 48 h at level 4 (~335 mb) are presented in Fig. 16. The term TA may be regarded as expressing the ventilation effect of the relative wind. The term TB consists of the effect of vertical

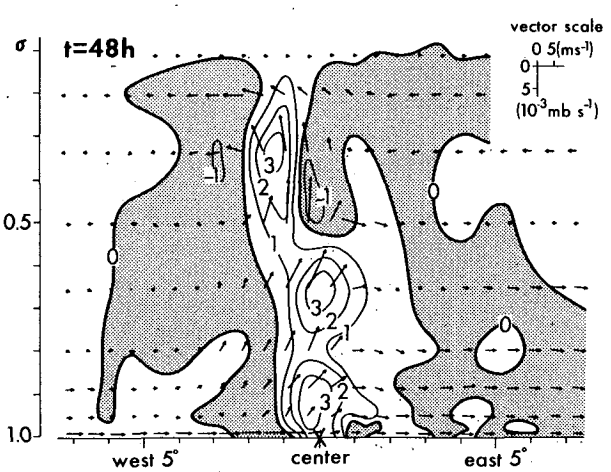

FIG. 15. Longitude-height distribution, through the disturbance center, of the rate of change of vorticity (10^{-9} s^{-2}), computed relative to the moving disturbance at 48 h. Arrows represent the zonal and vertical components of relative wind.

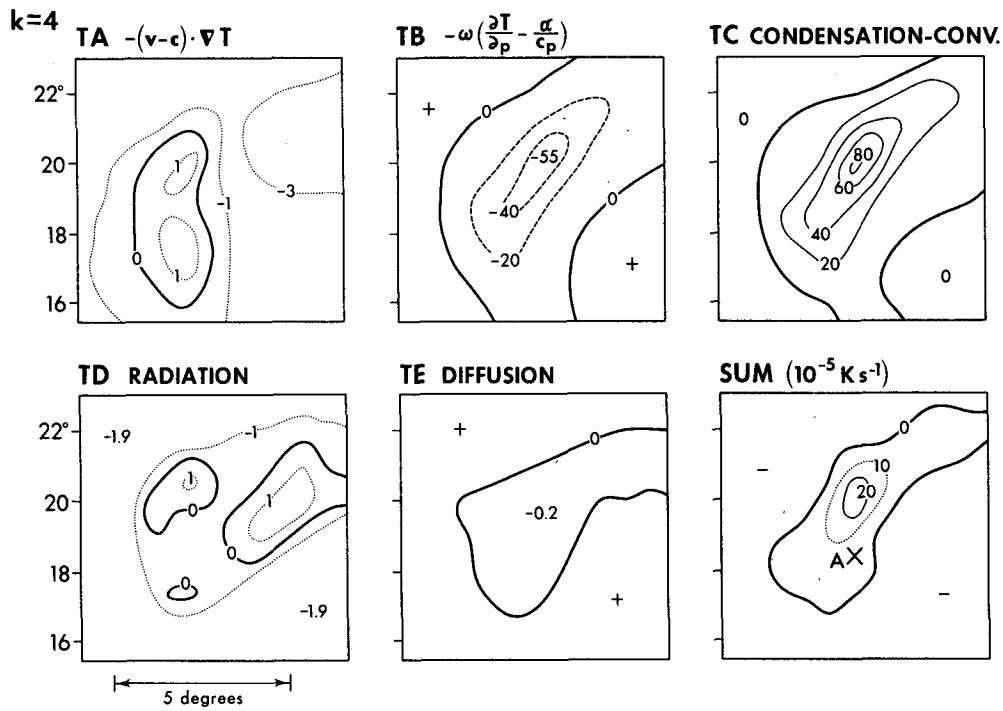

FIG. 16. Distribution of components and sum (10^{-5} K s^{-1}) of the heat budget at level 4, computed relative to the moving disturbance at 48 h. Cross mark in the lower right figure indicates surface position of disturbance A.

advection and the dry adiabatic change. In case of a stably stratified atmosphere, the upward motion yields negative TB, i.e., cooling. The zero-lines in the TB distribution indicate the boundaries between the areas of ascending and sinking motions. It is evident that the area of large negative TB corresponds to the region of positive TC, i.e., warming due to condensation-convection, with a larger magnitude. The radiation effect TD also gives a weak relative warming almost to the same area. The ventilation effect TA is as weak as the radiational effect. The positive tendency area in the TA distribution is caused by the relative outflow from the warm core toward the front of the depression. The net effect of the terms TA through TE produces the warming tendency in a small area which is contained in the region of ascending motion.

The zonal-vertical cross section of the sum of all heat budget terms is presented in Fig. 17. The warming tendency in the deep layer in front of the moving system is obtained. The warming results mainly from a delicate difference between the warming effect TC due to condensation-convection and the opposing cooling effect TB of upward motion. This is in agreement with the statement by Yanai (1964) on the warming stage of a tropical disturbance. Reed and Recker (1971) made the estimate of the rate of temperature change at the 500–400 mb level near the trough of a composite wave. Our net tendency shown in Fig. 17 is comparable to their estimate, i.e., ~6°C day^{-1}.

7. Transformation processes from a tropical depression to a tropical storm

The tropical disturbance simulated in our model deepens from 1006.4 mb (surface pressure minimum)

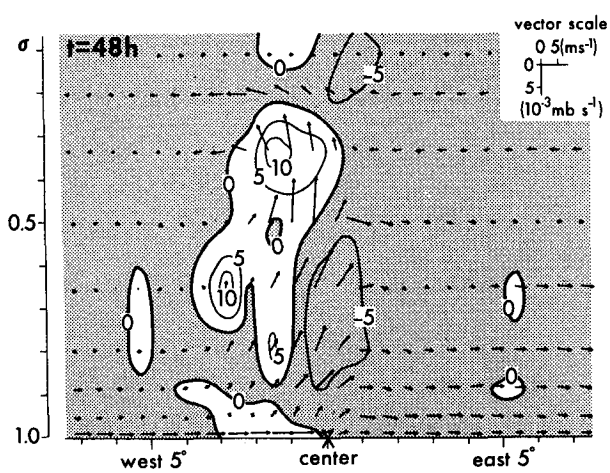

FIG. 17. Longitude-height distribution, through the disturbance center, of the rate of temperature change (10^{-5} K s^{-1}), computed relative to the moving disturbance at 48 h. See Fig. 15 for further information. (Magnitude is representative for this instant only. Fluctuations in values exist.)

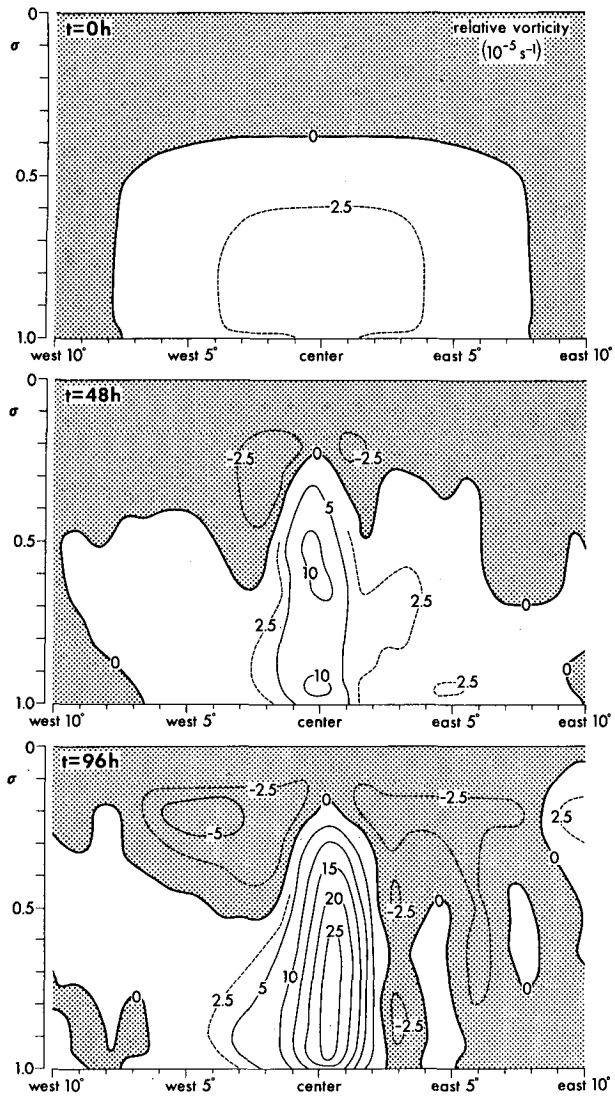

FIG. 18. Longitude-height distribution, through the disturbance center, of relative vorticity (10^{-5} s^{-1}) at 0 h (top), 48 h (middle) and 96 h (bottom).

and 12.5×10^{-5} s^{-1} (relative vorticity at level 9) at 48 h to 1002.6 mb and 23.7×10^{-5} s^{-1} at 96 h. The disturbance maintains the intensity of a tropical storm at 96 h. In this section, the structural change of the system during the above deepening period is discussed.

a. Intensification of a vortex

In Fig. 18, the zonal-vertical cross sections, through the center of the disturbance, of the relative vorticity at 0, 48 and 96 h are shown. The vortex column is well organized as it increases in intensity. At the lower levels, the positive vorticity area extends to the west of the storm at 96 h. At the upper levels, a large area of negative vorticity develops, into which the vortex column protrudes from below. The evolution of the vorticity field as mentioned above is consistent with the time sequence of the streamlines which is illustrated in Fig. 5.

b. Growth of a warm, moist core

As the vortex undergoes the above mentioned intensity change, its core becomes warmer. As a result, the dynamical balance condition or the thermal wind relation tends to be maintained.

In Fig. 19, the temperature deviation, which is obtained by subtracting the average of temperatures at 6° west and east of the center from the respective temperature along the latitude passing the center, at 96 h is compared against the same quantity at 48 h. At 48 h, the warm core is most pronounced at level 4 (~335 mb). There exists a cold core at level 3 (~215 mb). Evolution of those temperature fields was discussed in Section 5 (see Fig. 10). In the analysis of typhoon formation, Yanai (1961a) noticed the appearance of a warm core first at 300 mb and the existence of a cold core at a higher level. Fig. 19 shows the continued warming after 48 h at levels 4–7, making the downward extension of the warm core. The warming effect also propagates upward, probably through the vertical advection of warm air from below and the deep convection. As a result, the cold core

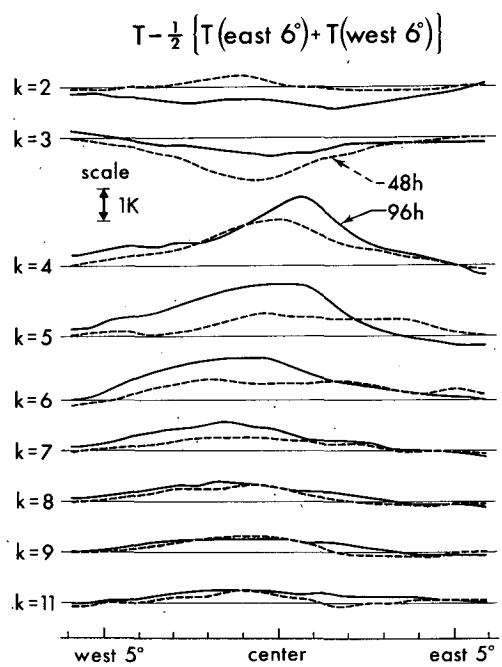

FIG. 19. Longitudinal distribution, through the disturbance center, of the temperature deviation from the average of those at 6° west and east, at different levels, at 48 h (dashed lines) and 96 h (solid lines).

at level 3 is weakened by 96 h. It is interesting to see the development of a relatively cold area at level 2 (~120 mb).

Next, we investigate the humidity field on a zonal-vertical cross section. Distributions of relative humidity and mixing ratio of water vapor at 0, 48 and 96 h are presented in Fig. 20. At the initial time, the relative humidity in the free atmosphere is below 80% everywhere. The field at 48 h shows the moistening of the central area between the 200 and ~600 mb levels. It is not very moist below 600 mb. In their composite wave analysis, Reed and Recker (1971) noted the departure from saturation in the trough region below 600 mb, with which our result agrees. At 96 h, a moist column extends from 200 to 700 mb with a forward tilt at the lower levels. Middle-level air in front of the above column is very dry. The outflow layer near 200 mb is characterized by a high relative humidity. In the boundary layer, the air to the east of the system is drier than the air near the system and to the west of it.

The growth of a warm, moist core indicates a decrease of conditional instability. In order to see the stability change, the equivalent potential temperature profiles at five locations including the system center at 48 and 96 h are drawn in Fig. 21. In the figure, the initial distribution is shown by dashed lines and the increase from the initial time is indicated by shading. A significant increase is seen only at the center and at 2.5° west. The change is gradual and the air column at any position is still conditionally unstable at 96 h. The change in the equivalent potential temperature in the present model is similar to the result of observational analysis obtained by Vincent and Waterman (1979).

c. *Some features of a tropical storm*

In Section 5, we examined the precipitation, cloud top, vertical motion and temperature fields during the early period of transformation of the disturbance (Figs. 9 and 10). The corresponding fields at 96 h are presented in Figs. 22 and 23. The pattern of rainfall and cloud distribution in Fig. 22 is blocklike and differs from a continuous zonal shape in the earlier period. The intense precipitation is obtained within a circular domain of 300 km diameter centered to the south-southeast of the storm center. It is associated with the tall cloud which reaches to level 3 (~215 mb). The maximum intensity of rainfall is 10.9 mm h^{-1}. In the other two areas, to the northeast and to the northwest of the primary one, the rainfall rate exceeds 2 mm h^{-1}. The cloud top in these areas is at level 4 (~335 mb).

Fig. 23, showing the fields of vertical velocity and temperature reveals a few interesting features. The strong upward motion near the storm center is obviously related to the primary rainfall.

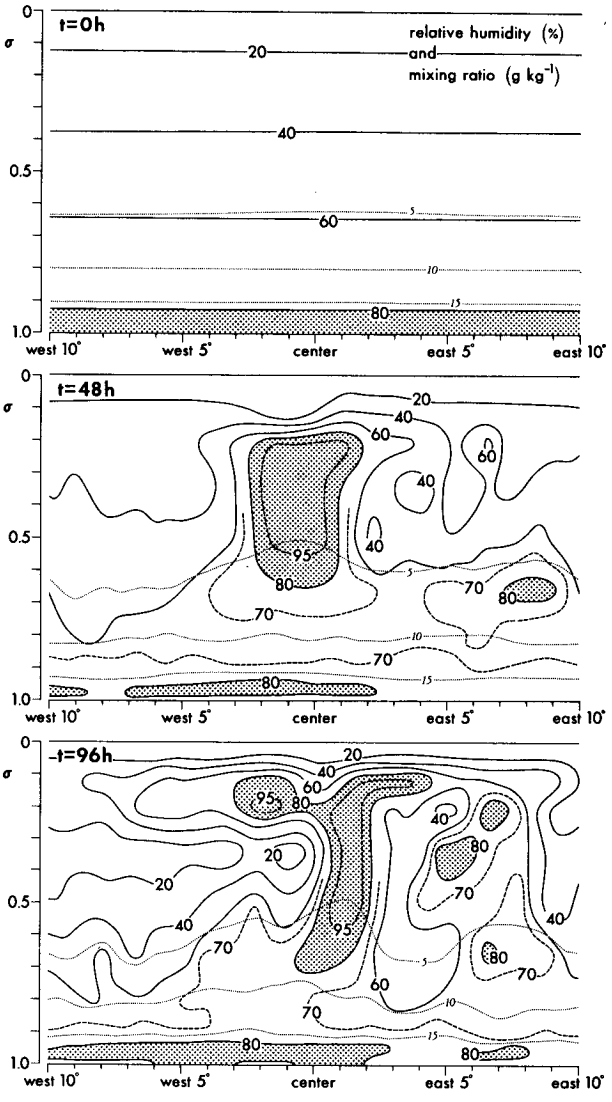

FIG. 20. Longitude-height distribution, through the disturbance center, of relative humidity (percent) and mixing ratio of water vapor (dotted lines, g kg^{-1}) at 0 h (top), 48 h (middle) and 96 h (bottom).

It extends to level 3, with an upward speed ~6 cm s^{-1} at level 7, ~10 cm s^{-1} at level 4, and ~2 cm s^{-1} at level 3. The warm core at level 4, which is compact and developed compared to the warm area in the earlier period, and the cold core at level 3 are situated at the area of the abovementioned ascending motion. There are two other maxima of upward motion, at level 7 (~800 mb) and at level 4 (~335 mb), but the maxima do not penetrate to level 3. The two secondary rainfall areas in Fig. 22 coincide with these areas of vertical motion. It should be noticed that neither a warm core nor a cold core is formed in these areas. The temperature field at level 4 is amazingly smooth compared to the field of ω. A similar feature is also found

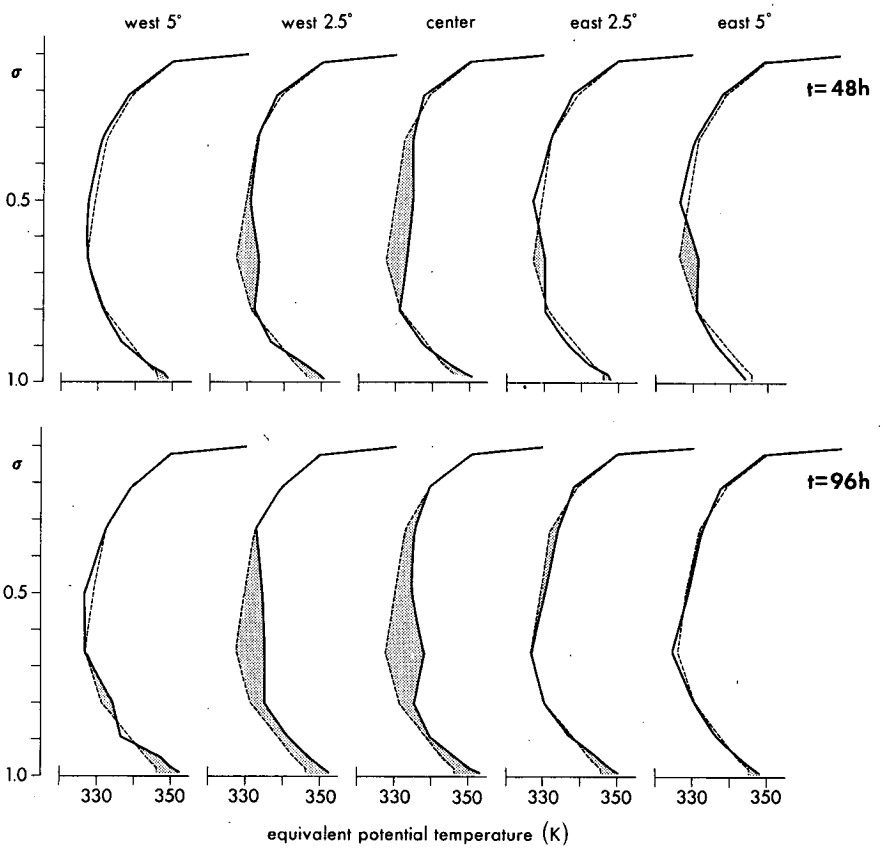

FIG. 21. Vertical variations of equivalent potential temperature (K) at the center of disturbance, 2.5° and 5° west and east, respectively, at 48 h (upper part) and 96 h (lower part). Dashed lines show the initial distribution and shading indicates the increase from the initial value.

at other levels. The warm area at level 7 was broad and weak at 36 h (Fig. 10). It is concentrated and well defined at 96 h. We note that the center of this warm area, the position of maximum upward motion at level 7 and the position of surface pressure minimum are different from each other.

8. Supplementary experiments to examine the effects of diabatic heating

In addition to the simulation experiment discussed so far (hereafter referred to as Exp. 1), we performed supplemental experiments in order to investigate the role of diabatic heating in the formation of tropical storms. The diabatic heating is related to three processes, i.e., radiative transfer, condensation of water vapor, and sensible heat exchange at the sea surface. In this study, the effects due to the first two processes are examined.

Differential radiative heating between cloud-free and overcast areas may affect disturbance intensification. As mentioned in Section 1, this effect was suggested by diagnostic study (Albrecht and Cox, 1975; Gray, 1979) as well as by numerical experiment using a prognostic model (Slingo, 1978). Fig. 24 shows the rate of radiative heating in the present model in a clear area and in an area where clouds are present at levels 2 (~120 mb) through 9 (~950 mb), respectively. The temperature changes shown in this figure are comparable to the estimates by Gray (1979, see Fig. 39). As indicated in Fig. 16, a relative warming due to radiation is expected in the region with strong convective activity. Another function of radiation is the destabilizing effect which is accomplished by the cooling of the air above the sea with a fixed surface temperature. This effect will oppose the stabilizing effect of cumulus convection. A third effect, which is not included in the present model, is associated with diurnally varying cloudiness. Krishnamurti *et al.* (1979) suggested the importance of this effect in the 3–4 day prediction of African disturbances. Usually, the radiational heating term itself is not large in the heat budget equation compared with some other terms as exemplified in Fig. 16. However, it will be shown that radiational heating may influence the efficiency of the energy transformation and affect the behavior of tropical disturbances.

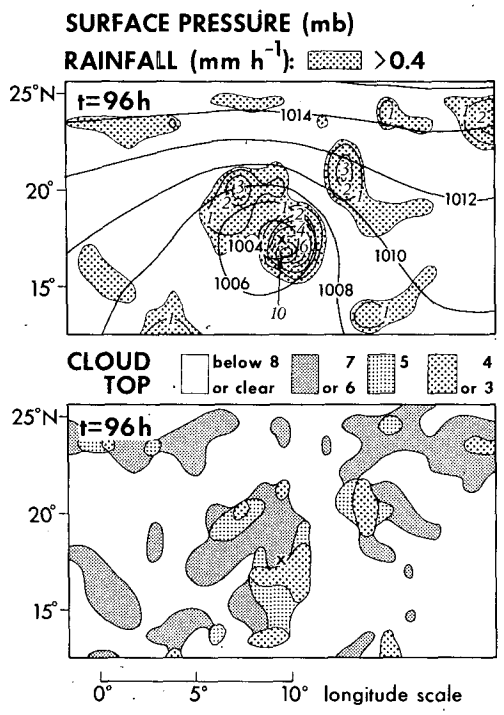

FIG. 22. Distribution of surface pressure (mb) and rainfall intensity (mm h^{-1}) (top) and level of cloud top (bottom) at 96 h. Location of surface pressure minimum is shown by cross mark.

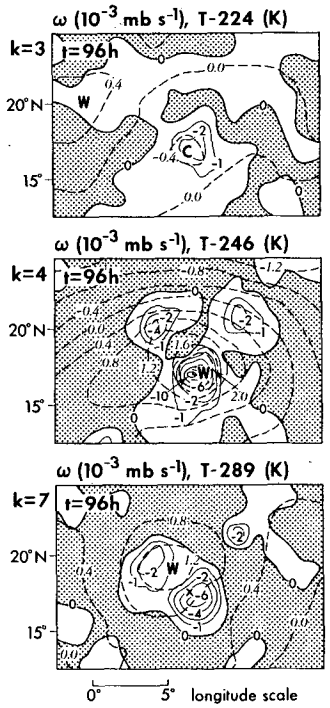

FIG. 23. Distribution of vertical p-velocity (10^{-3} mb s^{-1}, with shading for positive values) and deviation of temperature from appropriate value (dashed lines, K) at level 3 (top), 4 (middle) and 7 (bottom), at 96 h.

In Exp. 2, the time integration of the model is carried out without including the radiational effect. The time variation of the minimum surface pressure in this experiment is compared with that in Exp. 1 in Fig. 25. The rate of development is slow when the radiational heating is ignored. The maximum surface wind at 96 h is 13.8 m s^{-1} in Exp. 2, while it is 17.8 m s^{-1} in Exp. 1. If we include the radiational effect without taking cloudiness into consideration, then we can evaluate the overall destabilizing effect of radiation. A time integration of the model for such a case yields a development rate which is about halfway between Exps. 1 and 2. The above-mentioned destabilizing effect is as significant as the effect due to differential heating between cloudy and cloud-free areas. In Exp. 1, the radiational effect is entirely included. This seems to not only enhance the convective activity but also bring about the differential warming of the cloudy area. Thus, the development rate of the disturbance increases.

In Exp. 3, we further eliminate the hydrologic cycle from the model. In such a dry model, the initial disturbance does not develop as shown in Fig. 25, but rather decays. The maximum surface wind decreases from 9 m s^{-1} at 0 h to 7.3 m s^{-1} at 96 h. It seems that the hydrologic cycle is a prerequisite even in the formative stage of a tropical depression in the present model.

Wallace (1971) and Nitta (1972) argue that condensation heating is important in the energetics of the tropospheric wave disturbances in the western Pacific. The wave disturbance in this study is

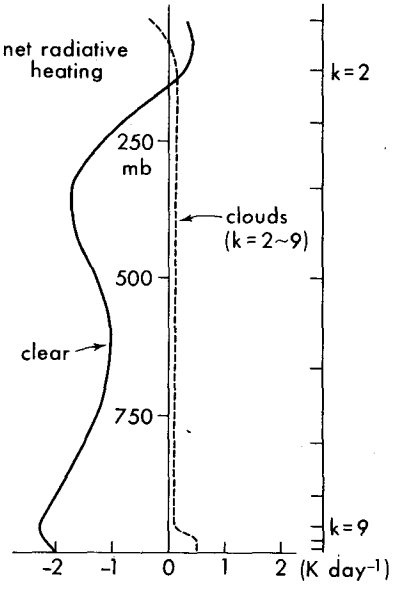

FIG. 24. Vertical distribution of net radiative heating rate (K day^{-1}) in clear area (solid line) and in an area with clouds at levels 2–9 (dashed line).

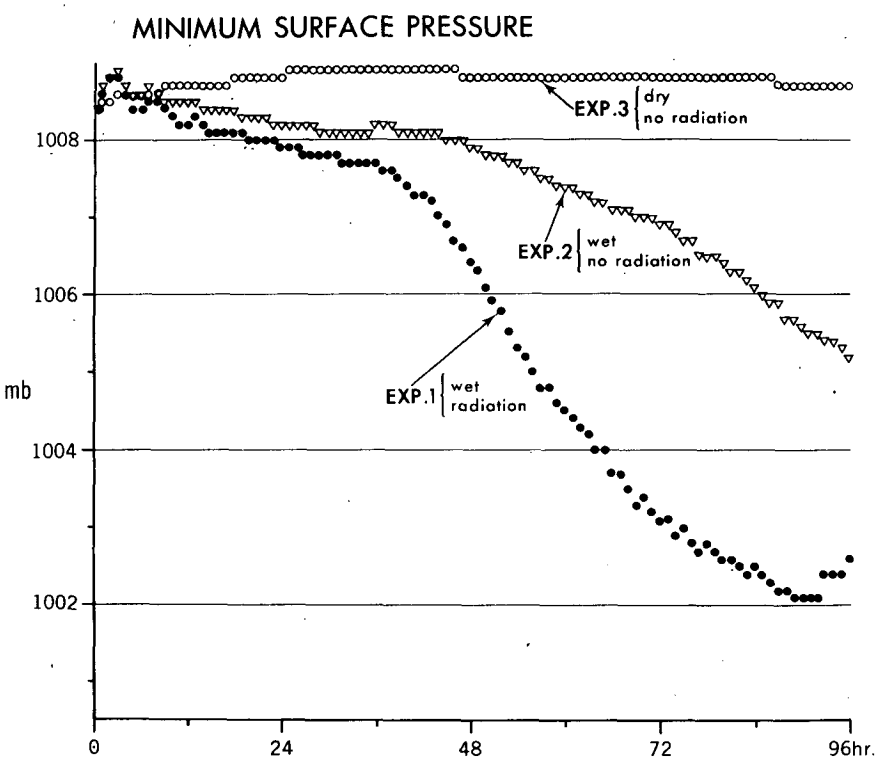

FIG. 25. Time variation of minimum surface pressure in Exps. 1, 2 and 3.

similar to a Pacific system in its energetics as well as in its initial structure. In contrast to the waves in the western Pacific, African waves may develop as a result of joint barotropic and baroclinic instability (Burpee, 1972). Norquist *et al.* (1977) suggest that, in addition to the above instability, the condensation process may also play a role in the energy transformation over Africa. The results of the energy analysis for Exp. 1 will be presented in a separate paper.

As mentioned in Section 3, the initial flow at the lower levels in the present model is barotropically unstable. This is manifested by the horizontal tilt of the wave axis after a few hours of time integration and the associated momentum transport. In case of the dry model (Exp. 3), the upward motion area is apparently correlated with the relatively cool area. This process of energy conversion from kinetic to potential energy is responsible for the decay of the disturbance. When the hydrologic cycle is added, i.e., in Exp. 2, the relative coolness of the rising air is moderated, and even a warm region appears. Then, the conversion from the eddy available potential to eddy kinetic energy may take place.

9. Summary and remarks

In the present numerical study, a case of the transformation of a shallow easterly wave into a deep vortex was simulated which provided information on the genesis mechanism of a tropical storm. During the above evolution, the minimum surface pressure of the disturbance dropped from 1008.4 mb to 1002.6 mb at 96 h. The relative vorticity at 950 mb intensified from 43×10^{-6} s^{-1} at the initial time to 237×10^{-6} s^{-1} at 96 h. The increase in the surface convergence was from 24×10^{-6} s^{-1} to 71×10^{-6} s^{-1}. The interesting features involved in the transformation of the system are the change in 1) rainfall and cloud distribution (an area of light rain and low-level cloud extending zonally north of the surface low at the beginning; persistent convective activity and the development of moderate rain and deep convection at and in front of the trough; extension of the moderate rain area to the west of the depression; intense rain and clustered clouds at the storm stage); 2) horizontal and vertical tilt of the trough axis (a north-northeast to south-southwest tilt at the wave stage; change of vertical tilt from eastward with increasing height in the early period to straight vertical at the depression stage); 3) vertical velocity (upward motion due to the boundary-layer convergence at the beginning; penetration of upward motion into higher levels); 4) depth of convergence layer (shallow layer at the beginning; thickening of convergence layer around the depression center), 5) area of relatively warm or cold temperature (appearance of a warm area at ~335 mb level and a

cold area above; continued warming and downward extension of a warm core during the development of the depression; upward propagation of warming effect and shift of cold area to a higher level), etc. In the present experiment, no disturbance system preexists at the upper levels. The evolution of the upper level disturbance in the present case is entirely a forced process from below. The present results, however, by no means rule out the possible importance of the upper level disturbance in the development of a tropical wave.

The vorticity budget analysis at the depression stage indicates that stretching of the vortex and relative horizontal advection are the major components of the vorticity tendency at low levels. At upper levels, the vertical advection and the twisting terms become important in addition to the above two effects. The net effect of vorticity budget is to produce a compact positive vorticity column.

The heat budget analysis shows that the formation of a warm core is mainly due to the condensation-convection heating which exceeds the cooling effect caused by the upward motion. The supplementary experiments suggest that the diabatic heating due to condensation of water vapor plays an essential role in the storm formation. The storm development is enhanced by the effect of radiation.

The time integration of the model was terminated at 96 h. We consider that a finer resolution than the present model is required in order to treat the development of a tropical storm into a hurricane or a typhoon. At any rate, whether the explosive deepening of the vortex occurs or not may depend on the establishment of a certain internal structure such as the inertial instability along isentropes (Yanai, 1961b).

The fundamental problem of tropical cyclone genesis is twofold, i.e., the dependency of genesis on the environmental condition and that on the state of the initial disturbance. The basic environmental field at the initial time in the present experiment was determined based on the observations at 80°W during the Phase III period of GATE. By the change in the basic flow, the superposed disturbance may behave differently. Comparative numerical experiments on this subject have been performed, and the analyses of the obtained results are under way. It should be noted here that these experiments proved the capability of the present model to simulate a non-developing case as well. The dependency of tropical storm genesis on the sea surface temperature is also being investigated.

The formation of tropical storms is one of the important issues in weather forecasting in the tropics. There may be two different ways, diagnostic and prognostic, in treating this problem. In a diagnostic approach, the potential for vortex intensification is evaluated in a given field with the use of appropriate criteria. As a guide along this line, Yanai (1963) derived an almost necessary and sufficient condition from the examination of many cases. Composite analysis (e.g., Gray, 1979) may serve to find out the meaningful meteorological parameters for this purpose. Combining the key quantities thus detected, a decision ladder or checklist to forecast storm formation has been made for a practical use (Hebert, 1978). Also, Shapiro (1977) proposed a genesis criterion based on the nonlinear dynamics of the wave. As described by Dvorak (1975), the analysis of satellite pictures is another technique to estimate tropical cyclone intensities.

It appears that the difficulty in the prediction of development or non-development of tropical disturbances is partly due to the undiscovery, or perhaps the lack of, a predominant, identifiable instability. The diversity of the formative process, especially at the early stage, adds to the difficulty. For instance, a certain parameter of the environmental condition may enhance the development in some cases and abort the growth potential in other cases, depending on the other parameters.

Under the above circumstances, the prognostic approach seems to be worthwhile persuing for the improvement of the forecast of tropical cyclogenesis. There are many problems to be solved in the use of numerical models. Initialization of a prediction model, including the problem of data acquisition, is one of them. Nevertheless, the experimental results from the primitive equation models obtained by Miller *et al.* (1972) and Ceselski (1974) are encouraging. In these experiments, both a developed system and a non-deepened system were treated. In addition to the usage mentioned above, a heuristic application of prognostic models can be suggested by the present study. Namely, if we define a certain basic meteorological state of the tropics, then we may be able to predict the evolution of an assumed disturbance which is hypothetically superposed on it. The obtained results may be utilized in the forecast of tropical storm genesis. Experiments are in progress to test the capability of the present model in such an application.

Acknowledgments. The authors would like to express their sincere appreciation to J. Smagorinsky and K. Miyakoda of the Geophysical Fluid Dynamics Laboratory for their constant encouragement during this study. They are also indebted to the colleagues in the Geophysical Fluid Dynamics Laboratory for their strong support and assistance, particularly to the members of the Climate Dynamics Project for their help in incorporating the radiation effect in the present model. The authors are grateful

to R. W. Burpee of the National Hurricane Research Laboratory for providing the needed data and making useful comments on the data. They wish to thank R. A. Anthes of the Pennsylvania State University, J. B. Hovermale of the National Meteorological Center, R. J. Reed of the University of Washington, and R. N. Keshavamurty, F. B. Lipps and K. Miyakoda of the Geophysical Fluid Dynamics Laboratory for valuable comments on the preliminary version of the manuscript. Thanks are also due to P. Tunison, W. Ellis, M. Zadworney, J. Conner and J. Kennedy, who assisted superbly in the preparation of the manuscript.

REFERENCES

Agee, E. M., 1972: Note on ITCZ wave disturbances and formation of Tropical Storm Anna. *Mon. Wea. Rev.*, **100**, 733–737.

Albrecht, B., and S. K. Cox, 1975: The large-scale response of the tropical atmosphere to cloud-modulated infrared heating. *J. Atmos. Sci.*, **32**, 16–24.

Burpee, R. W., 1972: The origin and structure of easterly waves in the lower troposphere of North Africa. *J. Atmos. Sci.*, **29**, 77–90.

——, 1974: Characteristics of North African easterly waves during the summers of 1968 and 1969. *J. Atmos. Sci.*, **31**, 1556–1570.

——, 1975: Some features of synoptic-scale waves based on compositing analysis of GATE data. *Mon. Wea. Rev.*, **103**, 921–925.

Ceselski, B. F., 1974: Cumulus convection in weak and strong tropical disturbances. *J. Atmos. Sci.*, **31**, 1241–1255.

Cochran, D. R., 1976: Unusual tropical development from a mid-Pacific cold low. *Mon. Wea. Rev.*, **104**, 804–808.

Colón, J. A., and W. R. Nightingale, 1963: Development of tropical cyclones in relation to circulation patterns at the 200 mb level. *Mon. Wea. Rev.*, **91**, 329–336.

Dickinson, R. E., and F. J. Clare, 1973: Numerical study of the unstable modes of a hyperbolic-tangent barotropic shear flow. *J. Atmos. Sci.*, **30**, 1035–1049.

Dunn, G. E., 1940: Cyclogenesis in the tropical Atlantic. *Bull. Amer. Meteor. Soc.*, **21**, 215–229.

Dvorak, V. F., 1975: Tropical cyclone intensity analysis and forecasting from satellite imagery. *Mon. Wea. Rev.*, **103**, 420–430.

Estoque, M. A., and C. S. Cheng, 1974: A theoretical study of tropical wave disturbances. *J. Meteor. Soc. Japan*, **52**, 106–119.

Fett, R. W., 1966a: Upper level structure of the formative tropical cyclone. *Mon. Wea. Rev.*, **94**, 9–18.

——, 1966b: Life cycle of tropical cyclone Judy as revealed by ESSA II and Nimbus 2. *Mon. Wea. Rev.*, **94**, 605–610.

Frank, N. L., 1963: Synoptic case study of tropical cyclogenesis utilizing TIROS data. *Mon. Wea. Rev.*, **91**, 355–366.

——, 1969: The "inverted V" cloud pattern—an easterly wave? *Mon. Wea. Rev.*, **97**, 130–140.

——, 1975: Atlantic tropical systems of 1974. *Mon. Wea. Rev.*, **103**, 294–300.

——, and G. Clark, 1979: Atlantic tropical systems of 1978. *Mon. Wea. Rev.*, **107**, 1035–1041.

Gray, W. M., 1968: Global view of the origin of tropical disturbances and storms. *Mon. Wea. Rev.*, **96**, 669–700.

——, 1979: Hurricanes: their formation, structure and likely role in the tropical circulation. *Meteorology over the Tropical Oceans*, D. B. Shaw, Ed., Roy Meteor. Soc., 155–218.

Hawkins, H. F., and D. T. Rubsam, 1968: Hurricane Hilda, 1964: I. Genesis, as revealed by satellite photographs, conventional and aircraft data. *Mon. Wea. Rev.*, **96**, 428–452.

Hayashi, Y., and D. G. Golder, 1978: The generation of equatorial transient planetary waves: Control experiments with a GFDL general circulation model. *J. Atmos. Sci.*, **35**, 2068–2082.

Hebert, P. J., 1978: Intensification criteria for tropical depressions of the western North Atlantic. *Mon. Wea. Rev.*, **106**, 831–840.

Hólton, J. R., 1971: A diagnostic model for equatorial wave disturbances: The role of vertical shear of the mean zonal wind. *J. Atmos. Sci.* **28**, 55–64.

Krishnamurti, T. N., and D. Baumhefner, 1966: Structure of a tropical disturbance based on solutions of a multilevel baroclinic model. *J. Appl. Meteor.*, **5**, 396–406.

——, H. L. Pan, C. B. Chan, J. Ploshay, D. Walker and A. W. Oodally, 1979: Numerical weather prediction for GATE. *Quart. J. Roy. Meteor. Soc.*, **105**, 979–1010.

Kurihara, Y., 1973: A scheme of moist convective adjustment. *Mon. Wea. Rev.*, **101**, 547–553.

——, and R. E. Tuleya, 1974: Structure of a tropical cyclone developed in a three-dimensional numerical simulation model. *J. Atmos. Sci.*, **31**, 893–919.

——, and G. J. Tripoli, 1976: An iterative time integration scheme designed to preserve a low-frequency wave. *Mon. Wea. Rev.*, **104**, 761–764.

——, and R. E. Tuleya, 1978: A scheme of dynamic initialization of the boundary layer in a primitive equation model. *Mon. Wea. Rev.*, **106**, 114–123.

——, and M. A. Bender, 1979: Supplementary note on "A scheme of dynamic initialization of the boundary layer in the primitive equation model." *Mon. Wea. Rev.*, **107**, 1219–1221.

——, and ——, 1980: Use of a movable nested-mesh model for tracking a small vortex. *Mon. Wea. Rev.*, **108**, 1792–1809.

Lacis, A. A., and J. E. Hansen, 1974: A parameterization for the absorption of solar radiation in the earth's atmosphere. *J. Atmos. Sci.*, **31**, 118–133.

Leary, C. A., and R. O. R. Y. Thompson, 1976: A warm-core disturbance in the western Atlantic during BOMEX. *Mon. Wea. Rev.*, **104**, 443–452.

Lipps, F. B., 1970: Barotropic stability and tropical disturbances. *Mon. Wea. Rev.*, **98**, 122–131.

Manabe, S., J. L. Holloway and H. M. Stone, 1970: Tropical circulation in a time-integration of a global model of the atmosphere. *J. Atmos. Sci.* **27**, 580–613.

Masuda, Y., 1978: A time integration scheme to damp efficiently high-frequency noises. *J. Meteor. Soc. Japan*, **56**, 571–583.

Mellor, G. L., and T. Yamada, 1974: A hierarchy of turbulence closure models for planetary boundary layers. *J. Atmos. Sci.*, **31**, 1791–1806.

Merritt, E. S., 1964: Easterly waves and perturbations, a reappraisal. *J. Appl. Meteor.*, **3**, 367–382.

Miller, B. I., P. P. Chase and B. R. Jarvinen, 1972: Numerical prediction of tropical weather systems. *Mon. Wea. Rev.*, **100**, 825–835.

Miyakoda, K., J. Sheldon and J. Sirutis, 1980: Four-dimensional analysis experiment with the GATE data. Part II. Submitted to *J. Atmos. Sci.*

——, L. Umscheid, D. H. Lee, J. Sirutis, R. Lusen and F. Pratte, 1976: The near-real-time, global, four-dimensional analysis experiment during the GATE period, Part I. *J. Atmos. Sci.*, **33**, 561–591.

Murakami, M., 1979: Large-scale aspects of deep convective activity over the GATE area. *Mon. Wea. Rev.*, **107**, 994–1013.

Nitta, Tsuyoshi, 1972: Energy budget of wave disturbances over

the Marshall Islands during the years of 1956 and 1958. *J. Meteor. Soc. Japan*, **50**, 71–84.

——, 1978: A diagnostic study of interaction of cumulus updrafts and downdrafts with large-scale motions in GATE. *J. Meteor. Soc. Japan*, **56**, 232–242.

——, and M. Yanai, 1969: A note on the barotropic instability of the tropical easterly current. *J. Meteor. Soc. Japan*, **47**, 127–130.

Norquist, D. C., E. E. Recker and R. J. Reed, 1977: The energetics of African wave disturbances as observed during Phase III of GATE. *Mon. Wea. Rev.*, **105**, 334–342.

Palmén, E. H., 1948: On the formation and structure of tropical hurricanes. *Geophysica*, **48**, 26–38.

Palmer, C. E., 1952: Tropical meteorology. *Quart. J. Roy. Meteor. Soc.*, **78**, 126–164.

Pedgley, D. E., and T. N. Krishnamurti, 1976: Structure and behavior of a monsoon cyclone over West Africa. *Mon. Wea. Rev.*, **104**, 149–167.

Perlroth, I., 1969: Effects of oceanographic media on equatorial Atlantic hurricanes. *Tellus*, **21**, 230–240.

Phillips, N. A., 1957: A coordinate system having some special advantages for numerical forecasting. *J. Meteor.*, **14**, 184–185.

Ramage, C. S., 1959: Hurricane development. *J. Meteor.*, **16**, 227–237.

Reed, R. J., 1979: The structure and behavior of easterly waves over West Africa and the Atlantic. *Meteorology over the Tropical Oceans*, D. B. Shaw, Ed., Roy. Meteor. Soc., 57–71.

——, and R. H. Johnson, 1974: The vorticity budget of synoptic-scale wave disturbances in the tropical western Pacific. *J. Atmos. Sci.*, **31**, 1784–1790.

——, D. C. Norquist and E. E. Recker, 1977: The structure and properties of African wave disturbances as observed during Phase III of GATE. *Mon. Wea. Rev.*, **105**, 317–333.

——, and E. E. Recker, 1971: Structure and properties of synoptic-scale wave disturbances in the equatorial western Pacific. *J. Atmos. Sci.*, **28**, 1117–1133.

Riehl, H., 1948: On the formation of typhoons. *J. Meteor.*, **5**, 247–264.

——, 1950: A model of hurricane formation. *J. Appl. Phys.*, **21**, 917–925.

——, 1954: *Tropical Meteorology*. McGraw Hill, 392 pp.

——, 1967: Varying structure of waves in the easterlies. *Dynamics of Large-Scale Atmospheric Processes*, Nauka, Moscow, 411–416.

Sadler, J. C., 1976: A role of the tropical upper tropospheric trough in early season typhoon development. *Mon. Wea. Rev.*, **104**, 1266–1278.

——, 1978: Mid-season typhoon development and intensity changes and the tropical upper tropospheric trough. *Mon. Wea. Rev.*, **106**, 1137–1152.

Schubert, W. H., J. J. Hack, P. L. Silva Dias and S. R. Fulton, 1980: Geostrophic adjustment in an axisymmetric vortex. *J. Atmos. Sci.*, **37**, 1464–1484.

Shapiro, L. J., 1977: Tropical storm formation from easterly waves: A criterion for development. *J. Atmos. Sci.*, **34**, 1007–1021.

——, 1978: The vorticity budget of a composite African tropical wave disturbance. *Mon. Wea. Rev.*, **106**, 806–817.

Shukla, J., 1969: A numerical experiment on a disturbance in the tropical easterlies. *J. Meteor. Soc. Japan*, **47**, 109–114.

Simpson, R. H., N. Frank, D. Shideler and H. M. Johnson, 1968: Atlantic tropical disturbances, 1967. *Mon. Wea. Rev.*, **96**, 251–259.

——, ——, —— and ——, 1969: Atlantic tropical disturbances of 1968. *Mon. Wea. Rev.*, **97**, 240–255.

Slingo, J. M., 1978: The effect of interactive clouds and radiation on convective activity in a numerical model of the tropics. *Workshop on the Parameterization of Cumulus Convection*, European Center for Medium Range Forecasts, 151–181.

Smagorinsky, J., 1963: General circulation experiments with the primitive equations: I. The basic experiment. *Mon. Wea. Rev.*, **91**, 99–164.

Stevens, D. E., 1979: Vorticity, momentum and divergence budgets of synoptic-scale wave disturbances in the tropical eastern Atlantic. *Mon. Wea. Rev.*, **107**, 535–550.

Thompson, O. E., and J. Miller, 1976: Hurricane Carmen: August–September, 1974—Development of a wave in the ITCZ. *Mon. Wea. Rev.*, **104**, 1194–1199.

Thompson, R. M., Jr., S. W. Payne, E. E. Recker and R. J. Reed, 1979: Structure and properties of synoptic-scale wave disturbances in the Intertropical Convergence Zone of the eastern Atlantic. *J. Atmos. Sci.*, **36**, 53–72.

Vincent, D. G., and R. G. Waterman, 1979: Large-scale atmospheric conditions during the intensification of Hurricane Carmen (1974). I. Temperature, moisture and kinematics. *Mon. Wea. Rev.*, **107**, 283–294.

Wallace, J. M., 1971: Spectral studies of tropospheric wave disturbances in the tropical western Pacific. *Rev. Geophys. Space Phys.*, **9**, 557–612.

Wendland, W. M., 1977: Tropical storm frequencies related to sea surface temperatures. *J. Appl. Meteor.*, **16**, 477–481.

Wetherald, R. T., and S. Manabe, 1980: Cloud cover and climate sensitivity. *J. Atmos. Sci.*, **37**, 1485–1510.

Yamasaki, M., and M. Wada, 1972a: Barotropic instability of an easterly zonal current. *J. Meteor. Soc. Japan*, **50**, 110–121.

——, and ——, 1972b: Vertical structure of the barotropic unstable wave in a tropical easterly current. *J. Meteor. Soc. Japan*, **50**, 271–284.

Yanai, M., 1961a: A detailed analysis of typhoon formation. *J. Meteor. Soc. Japan*, **39**, 187–214.

——, 1961b: Dynamical aspects of typhoon formation. *J. Meteor. Soc. Japan*, **39**, 282–309.

——, 1963: A preliminary survey of large-scale disturbances over the tropical Pacific region. *Geofis. Int.* **3**, 73–84.

——, 1964: Formation of tropical cyclones. *Rev. Geophys*, **2**, 367–414.

——, 1968: Evolution of a tropical disturbance in the Caribbean Sea region. *J. Meteor. Soc. Japan*, **46**, 86–109.